FINITE ELEMENT MODELLING AND MOLECULAR DYNAMIC SIMULATIONS

OF CARBON NANOTUBES/POLYMER COMPOSITES

A Thesis

by

DHATRI GADDAMANUGU

Submitted to the Office of Graduate Studies of
Texas A&M University
in partial fulfillment of the requirements for the degree of

MASTER OF SCIENCE

May 2009

Major Subject: Mechanical Engineering

FINITE ELEMENT MODELLING AND MOLECULAR DYNAMIC SIMULATIONS

OF CARBON NANOTUBES/POLYMER COMPOSITES

A Thesis

by

DHATRI GADDAMANUGU

Submitted to the Office of Graduate Studies of
Texas A&M University
in partial fulfillment of the requirements for the degree of

MASTER OF SCIENCE

Approved by:

Chair of Committee,   Junuthala N Reddy
Committee Members,   Jose Roesset
                        Xin Lin Gao
Head of the Department, Dennis L. O'Neal

May 2009

Major Subject: Mechanical Engineering

ABSTRACT

Finite Element Modelling and Molecular Dynamic Simulations of

Carbon Nanotubes/Polymer Composites. (May 2009)

Dhatri Gaddamanugu, B.E., Osmania University, India

Chair of Advisory Committee: Dr. Junuthala N. Reddy

Modeling of single-walled carbon nanotubes, multi-walled nanotubes and nanotube reinforced polymer composites using both the Finite Element method and the Molecular Dynamic simulation technique is presented. Nanotubes subjected to mechanical loading have been analyzed. Elastic moduli and thermal coefficient of expansion are calculated and their variation with diameter and length is investigated. In particular, the nanotubes are modeled using 3D elastic beam finite elements with six degrees of freedom at each node. The difficulty in modeling multi walled nanotubes is the van der Waal's forces between adjacent layers which are geometrically non linear in nature. These forces are modeled using truss elements. The nanotube-polymer interface in a nano-composite is modeled on a similar basis. While performing the molecular dynamic simulations, the geometric optimization is performed   initially to obtain the minimized configuration and then the desired temperature is attained by rescaling the velocities of carbon atoms in the nanotube. Results show that the Young's modulus increases with tube diameter in molecular mechanics whereas decreases in molecular dynamics since the inter-atomic potential due to chemical reactions between the atoms is taken into consideration in molecular dynamics unlike in molecular mechanics.

ACKNOWLEDGEMENTS

I would like to thank a few people whose whole hearted help made this work a reality. Firstly, I would like to thank my research advisor, Dr. J.N.Reddy, for his invaluable guidance all along the research work. I also thank Dr. Jose Roesset and Dr. Xin Lin Gao for being on my graduate committee and for extending support throughout the course of this research.

Thanks also go to all my friends and colleagues who have helped me in the successful completion of writing this thesis and the department faculty and staff for making my time at Texas A&M University a great experience. I also wish to thank Dr. Vinu Unnikrishnan for his help during the course of this study.

Finally, I sincerely thank all my family members for their encouragement, patience and love.

NOMENCLATURE

Å	Armstrong
CNT	Carbon Nanotube
DWCNT	Double Walled Carbon Nanotube
E	Young's modulus
FE	Finite Element
G	Shear modulus
MD	Molecular Dynamics
MM	Molecular Mechanics
MWCNT	Multi Walled Carbon Nanotube
MWNT	Multi Walled Nanotube
NVT	Constant Volume-Temperature
SWCNT	Single Walled Carbon Nanotube
SWNT	Single Walled Nanotube
α	Coefficient of Linear Expansion

TABLE OF CONTENTS

LIST OF FIGURES

FIGURE   Page

LIST OF TABLES

CHAPTER I

INTRODUCTION

Attempts have been made to study the mechanical behavior of SWNTs, MWNTs and subsequently nanotube embedded polymer composite subjected to various types of loads using both FE approach and atomistic approach (MD). One of the advantages of atomistic simulation is the ease with which various configurations can be studied when compared to an experimental investigation of CNT. The experimental investigation is extremely difficult as it is limited by the availability of high quality defect free CNTs of sufficient length and in the measurement of nanoscale objects. But due to the computational intensity both in terms of time and storage involved in carrying out MD simulations, there is a need to find an alternate computational methodology that prove to be accurate while correlating the nano-scale to macro-scale and allowing a thorough study of changing the properties of nanotube embedded polymer composites at macro level.

In the thesis, firstly, a three-dimensional finite element (FE) model of single-walled carbon nanotubes (SWCNTs) is presented. The model is based on the assumption that carbon nanotubes behave like space-frame structures. The bonds between carbon atoms are treated as connecting load-carrying members, while the carbon atoms as joints of the space frame. The elastic moduli of beam elements are determined by using a linkage between molecular mechanics and continuum mechanics. In order to evaluate the FE model and demonstrate its performance, the influence of tube wall thickness, diameter and chirality on

This thesis follows the style of Computer Methods in Applied Mechanics and Engineering.

the elastic moduli (Young's modulus and Shear modulus) of armchair SWCNTs is investigated. It is found that the choice of wall thickness significantly affects the calculation of Young's modulus. For the values of wall thickness used in the literature, the obtained values of Young's modulus agree very well with the corresponding theoretical results and many experimental measurements. Dependence of elastic moduli to diameter of the nanotubes is also obtained. With increase in tube diameter, the elastic moduli of the SWCNTs increases. The FE model developed herein may provide a valuable tool for studying the mechanical behavior of carbon nanotubes and their integration in nano-composites.

Secondly, a study of the elastic behavior of multi-walled carbon nanotubes (MWCNTs) is presented. The nested individual layers of an MWCNT are treated as single-walled frame-like structures and simulated by the molecular structural mechanics method. The interlayer van der Waals forces are represented through Lennard–Jones potential and simulated by a nonlinear truss -rod model. Results indicate that the tube diameter and number of tube layers have some noticeable effect on the elastic properties of MWCNTs. Furthermore, it has been demonstrated that the inner layers of an MWCNT can be effectively deformed only through the direct application of tensile or shear forces, not through van der Waals interactions. This is in the process of paving a way for the multi-scale modeling of the compressive behavior of carbon nanotube/polymer composites. The nanotube is modeled at the atomistic scale, and the matrix deformation is analyzed using the continuum based finite element model. The nanotube is modeled at the atomistic scale, and the matrix deformation is analyzed by the continuum finite element method. The

nanotube and polymer matrix are assumed to be bonded by van der Waals interactions at the interface leading us to examine the stress distributions at the nanotube/polymer interface and buckling behavior under compressive loading.

Finally, MD simulations of various SWNTs, MWNTs and a CNT polymer composite have been performed under different straining conditions at different temperatures using the PCFF force field. In the simulations, the entire systems have been minimized and later equilibrated for 1 ps (1000) steps. The temperature scale was carried out in 5 ps as an NVT ensemble (10,000) steps. During the minimization and NVT processes, the structures were placed in a unit cell and periodic boundary conditions were applied in all directions. All simulations have been made in Material Studio 4.3 (Accelrys inc.). Elastic constants have been calculated using the 'Forcite Mechanical Properties module' by stretching the periodic cell in one direction. The convergence plots and temperature variation have been presented for all the specimens considered. Variation of obtained values of Young's modulus and Shear modulus with tube diameter and length have been plotted to compare them with those obtained using FE method.

CHAPTER II

LITERATURE REVIEW

Carbon nanotubes (CNTs) are fullerenes, diamondoids, nano-onions and nanohorns discovered by Iijima in 1991 [1]. CNTs are nanometer-size cylinders made out of cylinder atoms. They can be thought of as a layer of graphite rolled up into a tube. Recently, individual single-walled carbon nanotubes (SWCNTs) and multi-walled carbon nanotubes (MWCNTs) were synthesized commercially.

Before full realization of the potential of the nanotechnologies in engineering applications, there is much work remaining to be done, such as good command of their physical properties and behaviors and well-controlled manipulation of the nanostructures to achieve desired material responses. In literature, extensive experimental studies using various advanced measurement tools with various nano-manipulation techniques have been carried out to identify the mechanical properties and behaviors of CNTs, including Young's modulus, Shear modulus, buckling behavior, and vibrational response. The earliest attempt to determine mechanical property of carbon nanotube was made by Treachy et al. [2]. Treachy et al. [2] estimated the Young's modulus of isolated nanotubes by measuring in the transmission electron microscope, the amplitude of their intrinsic thermal vibrations. They found out the average Young's modulus of individual nanotube to be 1.8 TPa. Subsequently, Wong et al. [3] determined the Young's modulus, strength and toughness of silicon carbide nanorods and multi-walled carbon nanotubes (MWCNTs) using atomic force microscopy. Tombler et al. [4] reported an experimental and theoretical elucidation of the electromechanical characteristics of individual single-walled carbon

nanotubes (SWNTs) under local-probe manipulation using atomic force microscope (AFM). Yu et al. [5] measured tensile strength of individual multi-walled carbon nanotubes (MWCNTs) with a nano stressing stage located within a scanning electron microscope and found that MWCNTs broke in the outer most layer and Young's modulus ranged from 11 to 63 GPa. Other relevant references regarding characterizing of CNTs can be found in Falvo et al. [6] and Krishnan et al. [7]. Inspite of all advancements in experimental techniques, characterization of mechanical behavior of nanomaterials poses great challenges from both physical and mechanical aspects. Mostly, due to cost insensitivity of experimentation hindered to gain the physical insights because of the microscopic dimensions of nanomatertials.

Computational approaches are typically more efficient and flexible as compared with experimental methods, and thus become a significant and powerful tool nowadays in the study of nanomaterials. Among the existing atomistic computational approaches, the classical MD simulation and the continuum modeling are two of the most widely-used techniques in nanomechanics (Shen and Atluri,[8]). Yakobson et al. [9] studied nanotubes under generic modes of axial compression, bending and torsion using molecular dynamics simulation. A remarkable synergism between the methods of MD and those of structural mechanics was found. The model provided remarkable good results of nanotube behavior beyond Hooke's law. Lu [10] investigated the elastic properties of carbon nanotubes and nanoropes using an empirical force-constant model. The simplicity of the model enables to explore the dependence of geometry on the properties of nanotubes and nanoropes.

Yao and Lodi [11] employed molecular dynamics using universal force field (UFF) to determined Young's modulus of single walled carbon nanotubes. They found out that

Young's modulus increases significantly with decreasing tube diameter. The effect of geometry (diameter and helicity) on Young's modulus is most pronounced for smaller tubes. Hernández et al. [12] carried out extensive structural, energetic and elastic properties of single walled carbon and composite nanotubes using a non-orthogonal tight binding formalism. The results indicate that graphitic nanotubes are stiffer than any of the composite nanotubes considered in this work, and that the elastic properties of single-wall nanotubes are of the same order of magnitude as those of the corresponding flat sheets. Jin and Yuan [13] studied the macroscopic mechanical behavior of the single walled carbon nanotube using molecular dynamics (MD) simulations in which the dynamic response and mutual force interaction among atoms of the nanostructures are obtained when subjected to small-strain deformation. Both force and energy approaches that link the behavior at the atomic and macroscopic scales of the nanotubes are used to predict the elastic moduli under different deformation modes. Xing et al. [14] studied the Young's moduli of armchair, zig-zag and chiral single walled carbon nanotubes based on molecular dynamics simulation where the inter-atomic short-range interaction and long-range interaction of carbon nanotubes are represented by a second generation reactive empirical bond order (REBO) potential and Lennard–Jones (LJ) potential, respectively. The computational results showed that the Young's moduli of SWCNTs are in the range of 929.8±11.5GPa. Liew et al. [15] carried out MD simulation in the micro-canonical ensemble to examine the elastic and plastic properties of single and multi-walled carbon nanotubes (CNTs) under axial tension. The interaction force between atoms is modeled using the second generation of reactive empirical bond order (REBO) potential coupled with Lennard Jones potential.

The MD simulation revealed that the fracture damage of MWCNTs takes place initially takes place in the outermost layer, and subsequently occurring in the inner layers.

Other references related to molecular dynamics simulation of CNTs can be found in, Gao et al.[16], Lier et al. [17] ,Zhou et al. [18] etc. Despite the powerful capability and great efficiency of microcomputers today, classical MD simulation is still limited to a relatively small-scale model, only containing atoms less than 10^6~10^8 and duration less than 10^{-6}~10^{-9} second. This has brought about the demand of more effective modeling techniques. One of the major developments is the so-called equivalent-continuum modeling (ECM) approach. It has been regarded as a very efficient method, especially for nano-structures with large scale, in contrast to MD simulation. Over the past years, many ECM models were presented in literature. For example, Ru [19] adopted an elastic shell model to study the buckling behaviors of double-walled CNTs. Odegard et al. [20] proposed a method which served as a link between computational chemistry and solid mechanics by substituting discrete molecular structures with equivalent-continuum models. The substitution is accomplished by equating the molecular potential energy of a nano-structured material with the strain energy of representative truss and continuum models. Li and Chou [21] studied the elastic behavior of multi-walled carbon nanotubes (MWCNTs) where the nested individual layers of MWCNT were treated as single-walled frame-like structures and simulated by the molecular structural mechanics method. The interlayer van der Waals forces were represented by Lennard–Jones potential and simulated by a nonlinear truss rod model. The computational results showed that the Young's moduli and shear moduli of MWCNTs are in the ranges of 1.05±0.05 and 0.40±0.05 TPa, respectively. Results indicated that the tube diameter, tube chirality and number of tube layers have

some noticeable effects on the elastic properties of MWCNTs Li and Chou [22] proposed structural mechanics approach to modeling of single-walled carbon nanotubes where CNT is space truss structure with C-C bond being modeled as load bearing beam and C atom as joints of load bearing beam. The proposed method was validated with existing theoretical and experimental results and revealed that both Young's modulus of both arm chair and zig-zag SWCNT increase with increasing tube diameter. In addition, Li and Chou [23-24] further applied the approach to investigate the vibrational and buckling behaviors of CNTs. Chang and Gao [25] derived closed form expressions for elastic modulus and Poisson's ratio as a function of the nanotube diameter based on the molecular mechanics approach. Properties at different length scales are directly connected via these expressions. Their study represented a preliminary effort to develop analytical methods of molecular mechanics for applications in nanostructure modeling. Natsuki et al. [26] derived closed form elastic solution based on a model of truss structures linked by inter-atomic potentials to predict elastic modulus, Poisson's ratio and deformation behavior of SWCNTs and MWCNTs. The studies showed that the disposition of the strain energy of bonds shows a quite a difference between zig-zag and armchair tubes subjected to axial loading and zigzag tubes have shown lower elongation property than an armchair tube. Natsuki and Endo [27] developed nanoscale continuum theory to directly incorporate the Morse potential function into the constitutive model of CNTs to simulate the stress strain behavior of carbon nanotube. The result showed that the armchair zigzag tube exhibits larger stress–strain response than the zigzag tube under tensile loading, but its relationship turns over between the tension and compression deformations. Natusuki et al. [28] developed a link analytical model based on a link between molecular and solid mechanics for the modeling

the elastic properties of single walled carbon nanotubes (SWCNTs). They regarded SWCNT as a continuum shell model which consisted of the discrete molecular structures linked by the carbon-to-carbon bonds and elastic properties where investigated on the based of nanotube size in terms of chiral vectors. Zhang et al. [29] investigated the elastic properties of two groups of SWCNTs by means of Tersoff-Bernner and modified Morse potentials based on Cauchy Born rule and brought out the fact that elastic modulus of SWCNTs depends dramatically on the tube radius ranging from 0.3-0.6 nm but not much on tube chirality. Xiao et al. [30] developed an analytical structural mechanics model for the prediction of defect free carbon nanotube by incorporating the modified Morse potential which capable of predicting Young's Moduli, Poisson's Ratio and stress-strain relationship carbon nanotube both under tensile and torsion loading condition. The model gave non-linear stress-strain relationship of CNTs which gives good approximation of ultimate strength and strain to the failures of nanotubes. Lau et al. [31] presented a critical review on the validity of different experimental and theoretical approaches to the mechanical properties of carbon nanotubes such measurement and modeling of tensile modulus, tensile strength, and torsional stiffness. Their studies put forth the fact the theoretical approaches such as molecular dynamic (MD) simulations, finite element analysis, and classical elastic shell theory were frequently used to analyze and interpret the mechanical features of carbon nanotubes gave inconsistent results due to the use of different fundamental assumptions and boundary conditions.

These ECM approaches have been proved effective and efficient, there are still some technical challenges remaining to be solved. Henceforth, molecular mechanics based finite element models have been employed to determine the mechanical response. For

instance, Sun and Zhao [32] used molecular mechanics based finite element approach to calculate tensile stiffness and strength of single walled carbon nanotube. Reported results reveal that the tensile stiffness was independent of nanotube diameter and helicity whereas Poisson's ratio was found to be dependent on nanotube diameter. Nanotube strength was predicted at 77–101GPa with the fracture strain around 0.3. Tserpes and Papanikos [33] developed a three dimensional finite element model based on the assumption that carbon nanotubes when subjected to loading behave like space frame structures to investigate the effect of geometry on the mechanical property of carbon nanotube. It was found that Young's modulus of chiral nanotube was greater than both armchair and zigzag nanotube. Meo and Rossi [34] evaluated the mechanical properties of single walled carbon nanotube based on finite element code on the use of non-linear and torsional spring elements. Use of spring elements in FE codes enabled to model the complex interaction of many atoms and also to model bond interaction without introduction of any non-physical variable such as area and inertia of atoms while using beam elements. Kalamkarov et al. [35] presented two different approaches to calculate the Young's modulus and Shear modulus of carbon nanotube. One approach consider carbon nanotubes as inhomogeneous cylindrical network shell using the asymptotic homogenization method and explicit formulae are derived for Young's modulus and Shear modulus of SWCNTs in terms pertinent material and geometric parameters. The second approach is based on finite element models where inter-atomic interactions due to covalent and non-covalent bonds are replaced by beam and spring elements respectively in the structural model. Giannopoulos et al. [36] proposed a three-dimensional finite element formulation for the computation of mechanical elastic response of armchair and zigzag SWCNTs for a wide range of values of nanotube's radius.

The linear elastic spring elements have been introduced in order to simulate the force field and inter-atomic interactions observed between the carbon atoms effectively. The advantage of the method is its simplicity and the fact that uses as input straightforwardly physical constants provided by molecular theory. Axial strain and torque loadings have been applied to compute the Young's modulus and Shear modulus of the SWCNTS, respectively.

CHAPTER III

THEORY: NANOSTRUCTURES

3.1 Atomic Structure of CNTs

There are two types of CNTs: SWCNTs and MWCNTs. MWCNTs are composed of co-axially situated SWCNTs of different radii. There are several ways to view a SWCNT. The most widely used is by reference to rolling up graphene sheet to form a hollow cylinder with end caps. The cylinder is composed of hexagonal carbon rings, while the end caps of pentagonal rings. The hexagonal pattern is repeated periodically leading to binding of each carbon atom to three neighboring atoms with covalent bonds. This covalent bond is a very strong chemical bond and plays significant role to the impressive mechanical properties of graphitic and as a consequence, of all carbon-related nano-structures. The atomic structure of nanotubes depends on tube chirality, which is defined by the chiral vector C_h and the chiral angle θ. The chiral vector is defined as the line connected from two crystallographic ally equivalently sites O and C on a two-dimensional graphene structure, as may be seen in Fig.3.1. The chiral vector C_h can be defined in terms of the lattice translation indices (n, m) and the basic vectors a_1 and a_2 of the hexagonal lattice (see Fig.3.1) as follows:
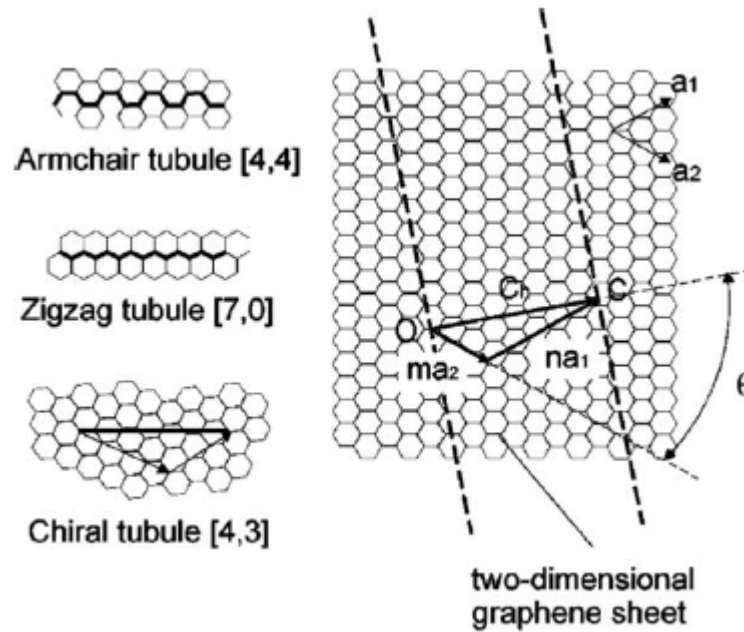
Fig 3.1 Schematic of the hexagonal lattice of graphene sheet including definition of basic structural parameters and explanation of SWCNTs formation [39].

$$\vec{C}_h = n\vec{a}_1 + m\vec{a}_2 \qquad\qquad (3.1)$$

The chiral angle θ is the angle between the chiral vector C_h with respect to the zigzag direction (n, 0) where θ=30° and the unit vectors a_1 and a_2. For the chiral angles of 0° and 30°, the armchair and zigzag nanotubes are formed, respectively. These two types of nanotubes correspond to the two limiting cases. In terms of the roll-up vector, the armchair nanotubes are defined by (n, n) and the zigzag nanotubes by (n, 0). For chiral angles different than 0° and 30°, the chiral nanotubes, which are defined by a pair of indices (n, m) are formed. Schematic representations of the three types of nanotubes are shown in Fig. 3.2.

3.2 Properties of CNTs

The mechanical properties are strongly dependent on the structure of the nanotubes. This is due to the high anisotropy of graphite. The single- and multi-wall nanotubes are interesting nanoscale materials for the following four reasons:

1. Single- and multi-wall nanotubes have very good elastomechanical properties because the two-dimensional arrangement of carbon atoms in a graphene sheet allows large out-of-plane distortions, while the strength of carbon-carbon in-plane bonds keeps the graphene sheet exceptionally strong against any in-plane distortion or fracture. These structural and material characteristics of nanotubes point towards their possible use in making next generation of extremely lightweight, but highly elastic, and very strong composite materials.

2. A single-wall nanotube can be either conducting or semiconducting, depending on its chiral vector (n, m), where n and m are two integers. The rule is that when the difference n-m is a multiple of three, a conducting nanotube is obtained. If the difference is not a multiple of three, a semiconducting nanotube is obtained. In addition, it is also possible to connect nanotubes with different chiralities creating nanotube hetero-junctions, which can form a variety of nanoscale molecular electronic device components.

3. Nanotubes, by structure, are high aspect-ratio objects with good electronic and mechanical properties. Consequently, the applications of nanotubes in field-emission displays or scanning probe microscopic tips for metrological purposes, have started to materialize even in the commercial sector.

4. Since nanotubes are hollow, tubular, caged molecules, they have been proposed as lightweight large surface area packing material for gas-storage and hydrocarbon fuel storage devices, and gas or liquid filtration devices, as well as nanoscale containers for molecular drug-delivery and casting structures for making nanowires and nanocapsulates.
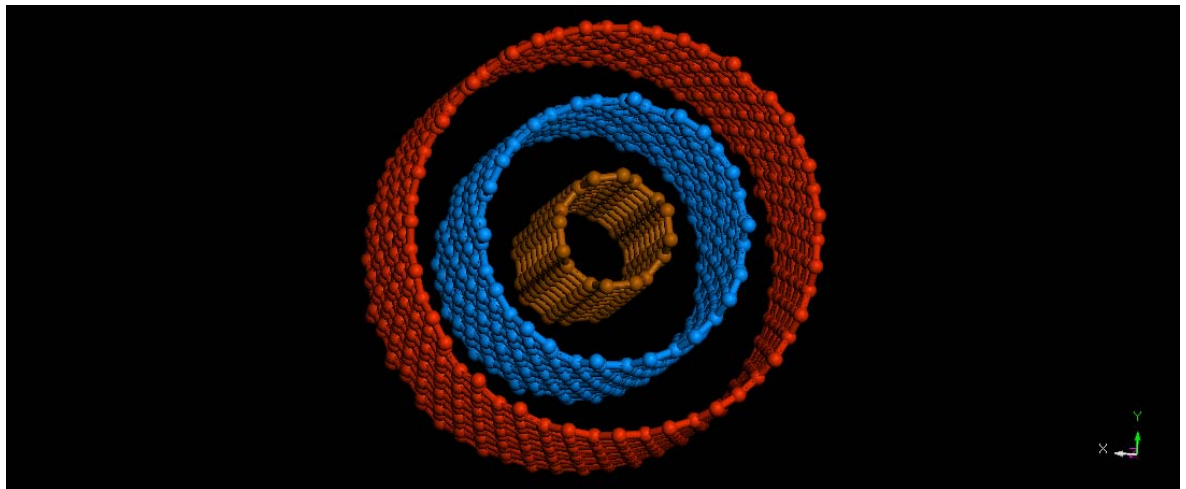
Fig 3.2 Multi walled nanotube with 3 layers

3.3 Applications of CNTs

CNTs have very unsual mechanical, chemical, thermal, electronic and optical properties, carbon nanotubes (CNTs) are promising to revolutionize several fields such a material science and nanotechnology. CNTs have wide range of unexplored potential applications in various technological areas such as aerospace , energy , automobile , medicine , or chemical industry, in which they can be used as gas absorbents, templates, actuators, composite reinforcements, catalyst supports, probes, chemical sensors, nanopipes, nanoreactors etc.

CHAPTER IV

FINITE ELEMENT FORMULATION OF 3D ELASTIC BEAM ELEMENTS

In this chapter, the finite element model for 3D elastic beam elements is described in a step by step manner as each bond in the nanotube is modeled using this element. 3D beam with six degrees of freedom at each node (3 translation + 3 rotation) is obtained by superposition of (i) 3D coupled Euler Bernoulli beam with coupling between axial displacement and rotation about orthogonal axis and (ii) Torsion element. Finite element equations of the two are derived individually from their respective governing differential equations.

4.1 3D Coupled Euler Bernoulli Beam

4.1.1 Displacement Field

The displacement field for Euler Bernoulli beam [40] having moderately large rotations but small strains is:

$$u_1 = u_0(x) - z\frac{dw_0(x)}{dx} - y\frac{dv_0(x)}{dx}, \ u_2 = v_0(x), \ u_3 = w_0(x) \tag{4.1}$$

(u_1, u_2, u_3) are the displacement along (x, y, z) axis and u_0, v_0 and w_0 are the are the axial displacement, transverse displacement in y direction and transverse displacement in z direction on the neutral axis, respectively. The following nonlinear strain-displacement relation is used to calculate the strains

$$\varepsilon_{ij} = \frac{1}{2}\left(\frac{\partial u_i}{\partial x_j} + \frac{\partial u_j}{\partial x_i}\right) + \frac{1}{2}\left(\frac{\partial u_m}{\partial x_i}\frac{\partial u_m}{\partial x_j}\right) \tag{4.2}$$

Substituting the values of u_1, u_2 and u_3 in the above equations and eliminating the large strain terms but retaining the rotation terms of the transverse normal we get,

$$\varepsilon_{11} = \varepsilon_{xx} = \frac{du_0}{dx} - z\frac{d^2 w_0}{dx^2} - y\frac{d^2 v_0}{dx^2} + \frac{1}{2}\left(\frac{dw_0}{dx}\right)^2 + \frac{1}{2}\left(\frac{dv_0}{dx}\right)^2$$

$$= \left[\frac{du_0}{dx} + \frac{1}{2}\left(\frac{dw_0}{dx}\right)^2 + \frac{1}{2}\left(\frac{dv_0}{dx}\right)^2\right] - y\left(\frac{d^2 v_0}{dx^2}\right) - z\left(\frac{d^2 w_0}{dx^2}\right) \tag{4.3}$$

$$= \varepsilon_{xx}^0 + y\varepsilon_{xx}^1 + z\tilde{\varepsilon}_{xx}^1$$

where, $\varepsilon_{xx}^0 = \left[\frac{du_0}{dx} + \frac{1}{2}\left(\frac{dw_0}{dx}\right)^2 + \frac{1}{2}\left(\frac{dv_0}{dx}\right)^2\right], \varepsilon_{xx}^1 = -\left(\frac{d^2 v_0}{dx^2}\right), \tilde{\varepsilon}_{xx}^1 = -\left(\frac{d^2 w_0}{dx^2}\right),$

These strains are known as *von Karman strains*.

4.1.2 Derivation of Governing Equations

According to the principle of virtual displacement, for a body in equilibrium, the virtual work done by the internal and external forces to move through their virtual displacements is zero. Thus based on this principle the following can be concluded.

$$\delta W^e \equiv \delta W_I^e + \delta W_E^e = 0 \tag{4.4}$$

where , δW_I^e is the virtual strain stored in the element due to σ_{ij} (Cartesian component of stress tensor) due to the virtual displacement $\delta \varepsilon_{ij}$ (Cartesian component of strain tensor) and δW_E^e is the work done by external forces. Thus for a beam element we have,

$$\delta W_I^e = \int_{V_e} \delta \varepsilon_{ij} \sigma_{ij} dV$$

$$\delta W_E^e = \int_{V_e} q_1 \delta v_0 dx + \int_{x_a}^{x_b} f \delta u_0 dx + \int_{V_e} q_2 \delta w_0 dx + \sum_{i=1}^{10} Q_i^e \delta \Delta_i^e \qquad (4.5)$$

where, V^e is the elemental volume, $q_1(x)$ is the distributed transverse load (per unit length) in y-direction, $q_2(x)$ is the distributed transverse load (per unit length) in z-direction and $f(x)$ distributed axial load. Q_i^e is the nodal force and $\delta \Delta_i^e$ is the nodal displacement of the element. The nodal displacements and nodal forces are

$$\Delta_1^e = u_0(x_a), \ \Delta_2^e = v_0(x_a), \Delta_3^e = w_0(x_a), \ \Delta_4^e = \left(-\frac{dv_0}{dx}\right)_{x_a} \equiv \theta_1(x_a), \Delta_5^e = \left(-\frac{dw_0}{dx}\right)_{x_a} \equiv \theta_2(x_a)$$

$$\Delta_6^e = u_0(x_b), \ \Delta_7^e = v_0(x_b), \ \Delta_8^e = w_0(x_b), \Delta_9^e = \left(-\frac{dv_0}{dx}\right)_{x_b} \equiv \theta_1(x_b), \Delta_{10}^e = \left(-\frac{dw_0}{dx}\right)_{x_b} \equiv \theta_2(x_b)$$

and
$$\begin{aligned} Q_1^e &= -N_{xx}(x_a), \quad Q_6^e = N_{xx}(x_b) \\ Q_2^e &= -\left[\frac{dv_0}{dx} N_{xx} + \frac{dM_{1xx}}{dx}\right]_{x_a}, \quad Q_7^e = \left[\frac{dv_0}{dx} N_{xx} + \frac{dM_{1xx}}{dx}\right]_{x_b} \\ Q_3^e &= -\left[\frac{dw_0}{dx} N_{xx} + \frac{dM_{2xx}}{dx}\right]_{x_a}, \quad Q_8^e = \left[\frac{dw_0}{dx} N_{xx} + \frac{dM_{2xx}}{dx}\right]_{x_b} \\ Q_4^e &= -M_{1xx}(x_a), \quad Q_9^e = M_{1xx}(x_b) \\ Q_5^e &= -M_{2xx}(x_a), \quad Q_{10}^e = M_{2xx}(x_b) \end{aligned} \qquad (4.6)$$

The virtual strain energy equation can be simplified by substituting equation (4.3) in equation (4.5) as follows:

$$\delta W_I^e = \int_{x_a}^{x_b} \int_{A^e} \delta \varepsilon_{xx} \sigma_{xx} \, dA \, dx$$

$$= \int_{x_a}^{x_b} \int_{A^e} \left(\delta \varepsilon_{xx}^0 + y \delta \varepsilon_{xx}^1 + z \delta \tilde{\varepsilon}_{xx}^1 \right) \sigma_{xx} \, dA \, dx$$

$$= \int_{x_a}^{x_b} \int_{A^e} \left[\left(\frac{d \delta u_0}{dx} + \frac{dv_0}{dx} \frac{d \delta v_0}{dx} + \frac{dw_0}{dx} \frac{d \delta w_0}{dx} \right) N_{xx} + M_{1xx} \left(\frac{d^2 \delta v_0}{dx^2} \right) + M_{2xx} \left(\frac{d^2 \delta w_0}{dx^2} \right) \right] dx \qquad (4.7)$$

where, N_{xx} is the axial force which can be expressed as $N_{xx} = \int_{A^e} \sigma_{xx} \, dA$ and M_{xx} is the

moment which can be expressed as $M_{1xx} = \int_{A^e} \sigma_{xx} y \, dA$, $M_{2xx} = \int_{A^e} \sigma_{xx} z \, dA$. Thus virtual

work statement can be written as

$$0 = \int_{x_a}^{x_b} \left[\left(\frac{d \delta u_0}{dx} + \frac{dv_0}{dx} \frac{d \delta v_0}{dx} + \frac{dw_0}{dx} \frac{d \delta w_0}{dx} \right) N_{xx} - M_{1xx} \left(\frac{d^2 \delta v_0}{dx^2} \right) - M_{2xx} \left(\frac{d^2 \delta w_0}{dx^2} \right) \right] dx$$

$$- \int_{V_e} q_1(x) \delta v_0(x) \, dx - \int_{V_e} q_2(x) \delta w_0(x) \, dx - \qquad (4.8)$$

$$\int_{x_a}^{x_b} f(x) \delta u_0(x) \, dx - \sum_{i=1}^{10} Q_i^e \delta \Delta_i^e$$

Collecting the coefficients of δu_0, δv_0 and δw_0 the following three equations are

obtained:

$$0 = \int_{x_a}^{x_b} \left[\left(\frac{d \delta u_0}{dx} N_{xx} - f(x) \delta u_0(x) \right) dx - Q_1^e \delta \Delta_1^e - Q_6^e \delta \Delta_6^e \right] dx$$

$$0 = \int_{x_a}^{x_b} \left[\frac{d \delta v_0}{dx} \left(\frac{dv_0}{dx} N_{xx} \right) - M_{1xx} \frac{d^2 \delta v_0}{dx^2} - q(x) \delta v_0(x) \right] dx - Q_2^e \delta \Delta_2^e - Q_3^e \delta \Delta_3^e - Q_7^e \delta \Delta_7^e - Q_8^e \delta \Delta_8^e \qquad (4.9)$$

$$0 = \int_{x_a}^{x_b} \left[\frac{d \delta w_0}{dx} \left(\frac{dw_0}{dx} N_{xx} \right) - M_{2xx} \frac{d^2 \delta w_0}{dx^2} - q(x) \delta w_0(x) \right] dx - Q_4^e \delta \Delta_4^e - Q_5^e \delta \Delta_5^e - Q_9^e \delta \Delta_9^e - Q_{10}^e \delta \Delta_{10}^e$$

Collecting the terms of δu_0, δv_0 and δw_0 and simplifying the terms,

$$\delta u_0: \qquad -\frac{dN_{xx}}{dx} = f(x)$$

$$\delta v_0: \qquad -\frac{d}{dx}\left(\frac{dv_0}{dx}N_{xx}\right) - \frac{d^2 M_{1xx}}{dx^2} = q_1(x) \qquad\qquad (4.10)$$

$$\delta w_0: \qquad -\frac{d}{dx}\left(\frac{dw_0}{dx}N_{xx}\right) - \frac{d^2 M_{2xx}}{dx^2} = q_2(x)$$

Thus the boundary conditions are:

$$Q_1^e + N_{xx}(x_a) = 0, \qquad\qquad Q_6^e - N_{xx}(x_b) = 0$$

$$Q_2^e + \left[\frac{dv_0}{dx}N_{xx} + \frac{dM_{1xx}}{dx}\right]_{x_a} = 0, \qquad Q_7^e - \left[\frac{dv_0}{dx}N_{xx} + \frac{dM_{1xx}}{dx}\right]_{x_b} = 0$$

$$Q_3^e + \left[\frac{dw_0}{dx}N_{xx} + \frac{dM_{2xx}}{dx}\right]_{x_a} = 0, \qquad Q_8^e - \left[\frac{dw_0}{dx}N_{xx} + \frac{dM_{2xx}}{dx}\right]_{x_b} = 0 \qquad (4.11)$$

$$Q_4^e + M_{1xx}(x_a) = 0, \qquad\qquad Q_9^e + M_{1xx}(x_b) = 0$$

$$Q_5^e + M_{2xx}(x_a) = 0, \qquad\qquad Q_{10}^e + M_{2xx}(x_b) = 0$$

4.1.3 Weak Form Development

Using the governing equations from equations (4.10) the weak form is developed as follows:

$$0 = \int_{x_a}^{x_b} v_1\left(-\frac{dN_{xx}}{dx} - f\right)dx$$

$$= \int_{x_a}^{x_b} \left(\frac{dv_1}{dx}N_{xx} - fv_1\right)dx - \left[v_1 N_{xx}\right]_{x_a}^{x_b}$$

$$= \int_{x_a}^{x_b} \left(\frac{dv_1}{dx}N_{xx} - fv_1\right)dx + v_1(x_a)N_{xx}(x_a) - v_1(x_b)N_{xx}(x_b)$$

$$(4.12a)$$

$$0 = \int_{x_a}^{x_b} v_2 \left[-\frac{d}{dx}\left(\frac{dv_0}{dx} N_{xx}\right) - \frac{d^2 M_{1xx}}{dx^2} - q_1 \right] dx$$

$$= \int_{x_a}^{x_b} \left[\frac{dv_2}{dx}\left(\frac{dv_0}{dx} N_{xx}\right) - \frac{d^2 v_2}{dx^2} M_{1xx} - q_1 v_2 \right] dx - \left[v_2 \left(\frac{dv_0}{dx} N_{xx} + \frac{dM_{1xx}}{dx}\right)\right]_{x_a}^{x_b} + \left[\left(\frac{dv_2}{dx}\right) M_{1xx}\right]_{x_a}^{x_b}$$

$$= \int_{x_a}^{x_b} \left[\frac{dv_2}{dx}\left(\frac{dv_0}{dx} N_{xx}\right) - \frac{d^2 v_2}{dx^2} M_{1xx} - q_1 v_2 \right] dx + v_2(x_a)\left[\left(\frac{dv_0}{dx} N_{xx} + \frac{dM_{1xx}}{dx}\right)\right]_{x_a}$$

$$- v_2(x_b)\left[\left(\frac{dv_0}{dx} N_{xx} + \frac{dM_{1xx}}{dx}\right)\right]_{x_b} + \left(\frac{dv_2}{dx}\right)_{x_b}\left[M_{1xx}(x_b)\right] - \left(\frac{dv_2}{dx}\right)_{x_a}\left[M_{1xx}(x_a)\right] \qquad (4.12b)$$

$$0 = \int_{x_a}^{x_b} v_3 \left[-\frac{d}{dx}\left(\frac{dw_0}{dx} N_{xx}\right) - \frac{d^2 M_{2xx}}{dx^2} - q \right] dx$$

$$= \int_{x_a}^{x_b} \left[\frac{dv_3}{dx}\left(\frac{dw_0}{dx} N_{xx}\right) - \frac{d^2 v_3}{dx^2} M_{2xx} - q v_3 \right] dx - \left[v_3 \left(\frac{dw_0}{dx} N_{xx} + \frac{dM_{2xx}}{dx}\right)\right]_{x_a}^{x_b} + \left[\left(\frac{dv_3}{dx}\right) M_{2xx}\right]_{x_a}^{x_b}$$

$$= \int_{x_a}^{x_b} \left[\frac{dv_3}{dx}\left(\frac{dw_0}{dx} N_{xx}\right) - \frac{d^2 v_3}{dx^2} M_{2xx} - q v_3 \right] dx + v_3(x_a)\left[\left(\frac{dw_0}{dx} N_{xx} + \frac{dM_{2xx}}{dx}\right)\right]_{x_a} - \qquad (4.12c)$$

$$- v_3(x_b)\left[\left(\frac{dw_0}{dx} N_{xx} + \frac{dM_{2xx}}{dx}\right)\right]_{x_b} + \left(\frac{dv_3}{dx}\right)_{x_b} M_{2xx}(x_b) - \left(\frac{dv_3}{dx}\right)_{x_a} M_{2xx}(x_a)$$

Here the weight functions are v_1, v_2 and v_3 are the weight functions which correspond to δu_0, δv_0 and δw_0 respectively. As mentioned in the assumptions earlier the EB has small to moderate rotations and the material is assumed to be linearly elastic which results in the following

$$\sigma_{xx} = E^e \varepsilon_{xx} \qquad (4.13)$$

The above relationship which defines the relationship between the total stress and the total strain is called as the Hooke's law. Thus we get

$$N_{xx} = \int_{A^e} \sigma_{xx} dA = \int_{A^e} E^e \varepsilon_{xx} dA$$

$$= \int_{A^e} E^e \left[\frac{du_0}{dx} + \frac{1}{2}\left(\frac{dv_0}{dx}\right)^2 + \frac{1}{2}\left(\frac{dw_0}{dx}\right)^2 \right] - y\left(\frac{d^2 v_0}{dx^2}\right) - z\left(\frac{d^2 w_0}{dx^2}\right) dA \tag{4.14}$$

$$= A_{xx}^e \left[\frac{du_0}{dx} + \frac{1}{2}\left(\frac{dv_0}{dx}\right)^2 + \frac{1}{2}\left(\frac{dw_0}{dx}\right)^2 \right]$$

$$M_{1xx} = \int_{A^e} \sigma_{xx} y dA = \int_{A^e} E^e \varepsilon_{xx} y dA$$

$$= \int_{A^e} E^e \left[\left[\frac{du_0}{dx} + \frac{1}{2}\left(\frac{dv_0}{dx}\right)^2 + \frac{1}{2}\left(\frac{dw_0}{dx}\right)^2 \right] - y\left(\frac{d^2 v_0}{dx^2}\right) - z\left(\frac{d^2 w_0}{dx^2}\right) \right] y dA = -D_{yy}^e \left(\frac{d^2 v_0}{dx^2}\right)$$

$$M_{2xx} = \int_{A^e} \sigma_{xx} z dA = \int_{A^e} E^e \varepsilon_{xx} z dA$$

$$= \int_{A^e} E^e \left[\left[\frac{du_0}{dx} + \frac{1}{2}\left(\frac{dv_0}{dx}\right)^2 + \frac{1}{2}\left(\frac{dw_0}{dx}\right)^2 \right] - y\left(\frac{d^2 v_0}{dx^2}\right) - z\left(\frac{d^2 w_0}{dx^2}\right) \right] z dA = -D_{xx}^e \left(\frac{d^2 w_0}{dx^2}\right)$$

where, A_{xx}^e is the extensional stiffness, B_{xx}^e is the extensional-bending stiffness and D_{xx}^e , D_{yy}^e are the bending stiffnesses. For isotropic material we have, $A_{xx}^e = E^e A^e$, and

$D_{xx}^e = \frac{1}{12} E^e bh^3$, $D_{yy}^e = \frac{1}{12} E^e hb^3$ where A^e is the cross section area and I^e is the second

moment of inertia of the beam element.

4.1.4 Finite Element Model

The interpolation functions for the axial and transverse deflection will be

$$u_0(x) = \sum_{j=1}^{2} u_j \psi_j(x) \quad v_0(x) = \sum_{j=1}^{4} \tilde{\Delta}_j \phi_j(x) \text{ and } \quad w_0(x) = \sum_{j=1}^{4} \overline{\Delta}_j \phi_j(x) \tag{4.15}$$

In the above equations ψ_j are Lagrange interpolation functions and ϕ_j are Hermite interpolation functions. Substituting the interpolation function in the weak form equation, the following equations are obtained:

$$0 = \sum_{j=1}^{2} K_{ij}^{11} u_j + \sum_{J=1}^{4} K_{iJ}^{12} \tilde{\Delta}_J + \sum_{k=1}^{4} K_{ik}^{13} \overline{\Delta}_k - F_i^1 \qquad (i = 1, 2)$$

$$0 = \sum_{j=1}^{2} K_{Ij}^{21} u_j + \sum_{J=1}^{4} K_{IJ}^{22} \tilde{\Delta}_J + \sum_{k=1}^{4} K_{IJ}^{23} \overline{\Delta}_k - F_I^2 \qquad (I = 1, 2, 3) \qquad (4.16)$$

$$0 = \sum_{j=1}^{2} K_{Ij}^{31} u_j + \sum_{J=1}^{4} K_{IJ}^{32} \tilde{\Delta}_J + \sum_{k=1}^{4} K_{Ik}^{33} \overline{\Delta}_k - F_k^3 \qquad (k = 1, 2, 3)$$

where,

$$K_{11} = \int_{x_a}^{x_b} A_{xx}^e \frac{d\psi_i}{dx} \frac{d\psi_j}{dx} dx, \quad K_{12} = \frac{1}{2} \int_{x_a}^{x_b} A_{xx}^e \frac{dv_0}{dx} \frac{d\psi_i}{dx} \frac{d\phi_j}{dx} dx, \quad K_{13} = \frac{1}{2} \int_{x_a}^{x_b} A_{xx}^e \frac{dw_0}{dx} \frac{d\psi_i}{dx} \frac{d\phi_j}{dx} dx$$

$$K_{21} = \int_{x_a}^{x_b} A_{xx}^e \frac{dv_0}{dx} \frac{d\phi_i}{dx} \frac{d\psi_j}{dx} dx,$$

$$K_{22} = \int_{x_a}^{x_b} \left(A_{xx}^e \left(\frac{dv_0}{dx} \right)^2 \frac{d\phi_I}{dx} \frac{d\phi_J}{dx} + D_{yy}^e \frac{d^2\phi_I}{dx^2} \frac{d^2\phi_J}{dx^2} \right) dx, \quad K_{23} = \int_{x_a}^{x_b} \left(A_{xx}^e \left(\frac{dw_0}{dx} \right) \left(\frac{dv_0}{dx} \right) \frac{d\phi_I}{dx} \frac{d\phi_J}{dx} \right) dx$$

$$K_{31} = \int_{x_a}^{x_b} A_{xx}^e \frac{dw_0}{dx} \frac{d\phi_I}{dx} \frac{d\psi_j}{dx} dx, \quad K_{32} = \int_{x_a}^{x_b} \left(A_{xx}^e \frac{dv_0}{dx} \frac{dw_0}{dx} \frac{d\phi_I}{dx} \frac{d\phi_J}{dx} \right) dx,$$

$$K_{33} = \int_{x_a}^{x_b} \left(A_{xx}^e \frac{1}{2} \left(\frac{dw_0}{dx} \right)^2 \frac{d\phi_I}{dx} \frac{d\phi_J}{dx} + D_{xx}^e \frac{d^2\phi_I}{dx^2} \frac{d^2\phi_J}{dx^2} \right) dx$$

$$F_i^1 = \int_{x_a}^{x_b} f\psi_i\,dx + Q_i$$

$$F_I^2 = \int_{x_a}^{x_b} q_1\phi_I\,dx + \tilde{Q}_I \qquad (4.17)$$

$$F_J^3 = \int_{x_a}^{x_b} q\phi_J\,dx + \bar{Q}_J$$

In matrix form it can be written as

$$\begin{pmatrix} [K_{11}] & [K_{12}] & [K_{13}] \\ [K_{11}] & [K_{11}] & [K_{23}] \\ [K_{11}] & [K_{11}] & [K_{33}] \end{pmatrix} \begin{Bmatrix} \{u_j\} \\ \{\tilde{\Delta}\} \\ \{\bar{\Delta}\} \end{Bmatrix} = \begin{Bmatrix} \{F^1\} \\ \{F^2\} \\ \{F^3\} \end{Bmatrix} \qquad (4.18)$$

4.2. Torsion Element

In this section, the torsion element is introduced in order to model the twist of C-C bonds, The governing differential equation of torsion[41] is given by

$$-\frac{d}{dx}\left(GJ\frac{du}{dx}\right) = f(x) \qquad (4.19)$$

The weak form is given by the following

$$0 = \int_{x_a}^{x_b}\left[-\frac{dw}{dx}\left(GJ\frac{du}{dx}\right) - fw\right]dx - \left[wGJ\frac{du}{dx}\right]_a^b \qquad (4.20)$$

The finite element equations obtained by substituting the approximation function are

$$\left[K^e \right] = GJ \begin{pmatrix} 1 & -1 \\ -1 & 1 \end{pmatrix}$$

$$\left[F^e \right] = \frac{f}{2} \begin{Bmatrix} 1 \\ 1 \end{Bmatrix}$$

(4.21)

Thus, the left over dof i.e. rotation in x-direction is obtained.

Superposing the above two different elements to get the 6 DOF (3 translation and 3 rotation) at each node, the total non-linear stiffness matrix for the 3D elastic beam element is derived.

In contrast, Li and Chou [22] used the linear stiffness matrix by superposing a bar and torsion element for translation and rotation in x-direction, two 2D Euler-Bernoulli beams in perpendicular directions to obtain translations and rotations in y and z directions and so the total stiffness matrix becomes

$$K = \begin{pmatrix} K_{ii} & K_{ij} \\ K_{ij}^T & K_{jj} \end{pmatrix} \quad \text{where,}$$

(4.22)

$$K_{ii} = \begin{bmatrix}
EA/L & 0 & 0 & 0 & 0 & 0 \\
0 & 12EI_x/L^3 & 0 & 0 & 0 & 6EI_x/L^2 \\
0 & 0 & 12EI_y/L^3 & 0 & -6EI_y/L^2 & 0 \\
0 & 0 & 0 & GJ/L & 0 & 0 \\
0 & 0 & -6EI_y/L^2 & 0 & 4EI_y/L & 0 \\
0 & 6EI_x/L^2 & 0 & 0 & 0 & 4EI_x/L
\end{bmatrix}$$

$$K_{ij} = \begin{bmatrix}
-EA/L & 0 & 0 & 0 & 0 & 0 \\
0 & -12EI_x/L^3 & 0 & 0 & 0 & 6EI_x/L^2 \\
0 & 0 & -12EI_y/L^3 & 0 & -6EI_y/L^2 & 0 \\
0 & 0 & 0 & -GJ/L & 0 & 0 \\
0 & 0 & -6EI_y/L^2 & 0 & 2EI_y/L & 0 \\
0 & -6EI_x/L^2 & 0 & 0 & 0 & 2EI_x/L
\end{bmatrix}$$

$$K_{jj} = \begin{bmatrix} EA/L & 0 & 0 & 0 & 0 & 0 \\ 0 & 12EI_x/L^3 & 0 & 0 & 0 & -6EI_x/L^2 \\ 0 & 0 & 12EI_y/L^3 & 0 & 6EI_y/L^2 & 0 \\ 0 & 0 & 0 & GJ/L & 0 & 0 \\ 0 & 0 & 6EI_y/L^2 & 0 & 4EI_y/L & 0 \\ 0 & -6EI_x/L^2 & 0 & 0 & 0 & 4EI_x/L \end{bmatrix}$$

The elemental equilibrium equation can be written as

$$Ku = f, \tag{4.23}$$

where, $u = [u_{xi}, u_{yi}, u_{zi}, \theta_{xi}, \theta_{yi}, \theta_{zi}, u_{xj}, u_{yj}, u_{zj}, \theta_{xj}, \theta_{yj}, \theta_{zj}]^T$,

$$f = [f_{xi}, f_{yi}, f_{zi}, m_{xi}, m_{yi}, m_{zi}, f_{xj}, f_{yj}, f_{zj}, m_{xj}, m_{yj}, m_{zj}]^T$$

In order to obtain the deformation of a space frame, the above elemental stiffness equations should be established for every element in the space frame and then all these equations should be transformed from the local coordinates to a common global reference system. Finally, a system of simultaneous linear equations can be assembled according to the requirements of nodal equilibrium. By solving the system of equations and taking into account the boundary restraint conditions, the nodal displacements are obtained.

CHAPTER V

FINITE ELEMENT MODELING OF SINGLE-WALLED, MULTI-WALLED CARBON

NANOTUBES AND POLYMER COMPOSITES

5.1. Finite Element Modeling of Single Walled Nanotube

A three-dimensional finite element (FE) model for armchair (5,5) single-walled carbon nanotubes (SWCNTs) is presented. The model development is based on the assumption that carbon nanotubes, when subjected to loading, behave like space-frame structures. The bonds between carbon atoms are considered as connecting load-carrying members, while the carbon atoms as joints of the members. To create the FE models, nodes are placed at the locations of carbon atoms and the bonds between them are modeled using three-dimensional elastic beam elements. The elastic moduli of beam elements are determined by using a linkage between molecular and continuum mechanics.

5.1.1 Aim

To evaluate the FE model and demonstrate its performance, the influence of tube wall thickness, diameter and chirality on the elastic moduli (Young's modulus, Shear modulus, coefficient of thermal expansion in radial and axial direction) of SWCNTs is investigated.

5.1.2 3D FE Model Development Using ANSYS

Bonds are modeled using 3D ELASTIC BEAM4 element [37]. The specific element is a uni-axial element with tension, compression, torsion and bending capabilities.

As described in chapter 4, it has six degrees of freedom at each node: translations in the nodal x, y, and z directions and rotations about the nodal x, y, and z-axes. The element is defined by two nodes as well as its cross-sectional area, two moments of inertia, two dimensions and the material properties. Fig.5.1 depicts how the hexagon, which is the constitutional element of CNTs nano-structure, is simulated as structural element of a space-frame. In the same way the entire nanotube lattice is simulated. The simulation leads to the correspondence of the bond length a C–C with the element length L as well as the wall thickness t with the element thickness. By assuming a circular cross-sectional area for the element, as in Fig.5.1, t corresponds to the element diameter d.
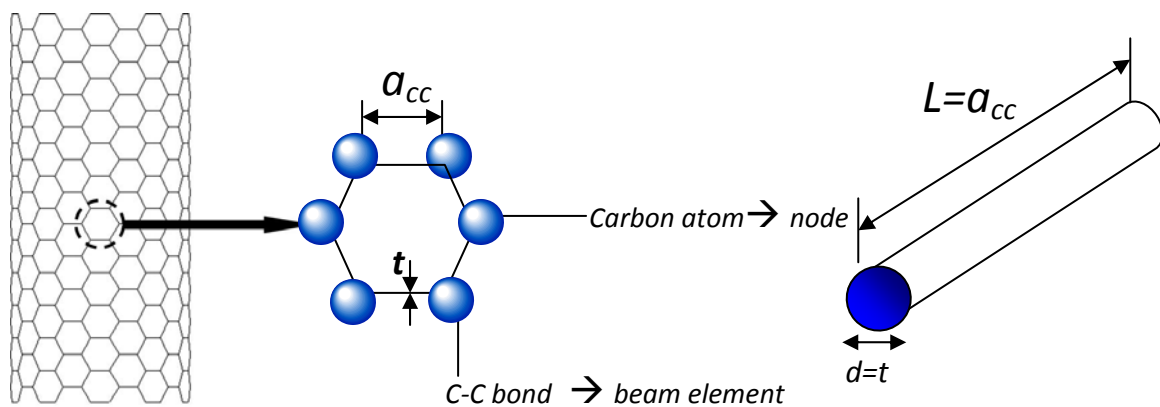

Fig 5.1 Simulation of a SWCNT as a space-frame structure

5.1.3 Relationship between Material Stiffness Parameters and the Constants of Force Fields

Presently, there is no information about the material and sectional properties of the C-C bonds under the theory of continuum mechanics. Therefore it is indispensable to establish a relationship between the theory of nano-scale mechanics and the theory of continuum mechanics. The best way to analyze the nano-scale mechanics is MD

simulation. The Tersoff-Brenner force field is the foundation of MD simulation, and the force field is generated owing to the interaction of the atoms-atoms, which regulates the motion of the atoms in a molecule. Usually, the inter-atomic interactions in molecular mechanics of a molecular structure can be described as five forms below: bond stretching, bond angle bending, improper (out-of-plane) torsion and dihedral angle torsion and van-der Waals force, as shown in Fig.5.2.
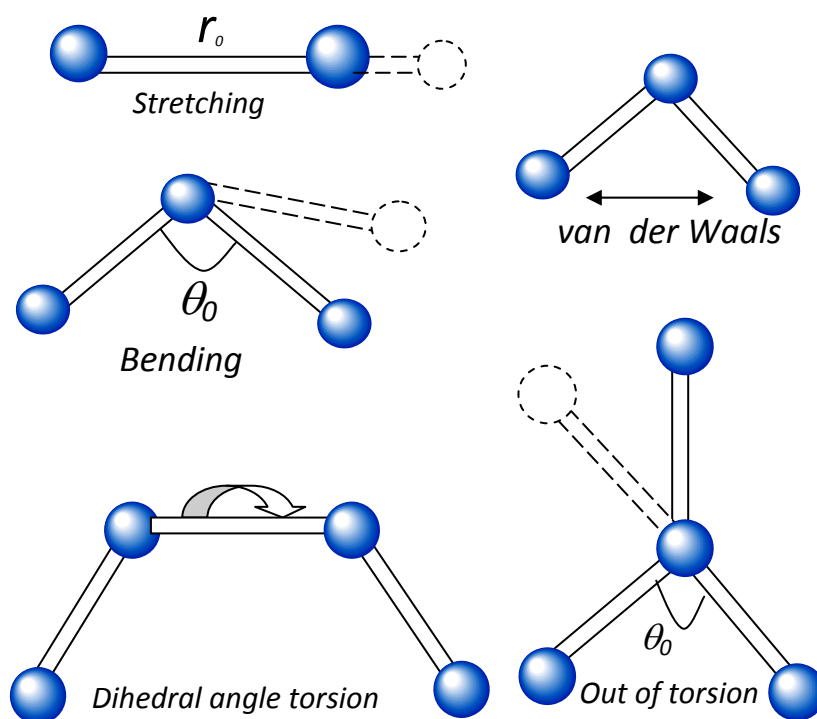

Fig 5.2 Inter-atomic interactions in molecular mechanics

According to the Tersoff-Brenner force field, the general expression of the total steric potential energy is the sum of energies due to valence or bonded interaction and non-bonded interaction:

$$U = U_r + U_\theta + U_\phi + U_\omega + U_{vdw} \tag{5.1}$$

where, U_r is the potential energy induced by the bond stretch interaction, U_θ by the bond angle bending, U_φ by the dihedral angle torsion, U_ω by the improper (out-of-plane) torsion, U_{vdw} by the non-bonded van der-Waals interaction. It is clear that the energy associated with van der Waals interactions is highly nonlinear with respect to inter-atomic distance and much less than the other bond energy. So in the present analysis, the effect of vander Waals interaction is neglected. And for simplicity and convenience, the simplest harmonic forms are adopted, with the dihedral angle torsion and the improper torsion merged into a single equivalent term, i.e.

$$U_r = \tfrac{1}{2}K_r \left(r - r_0 \right)^2 = \frac{1}{2}K_r \left(\Delta r \right)^2 \tag{5.2}$$

$$U_\theta = \tfrac{1}{2}K_\theta \left(\theta - \theta_0 \right)^2 = \frac{1}{2}K_\theta \left(\Delta \theta \right)^2 \tag{5.3}$$

$$U_r = U_\Phi + U_\omega = \frac{1}{2}K_r \left(\Delta \Phi \right)^2 \tag{5.4}$$

where K_r, K_θ and $K\tau$ are the bond stretching force constant, bond angle bending force constant and torsional resistance, respectively, and the symbols Δr, $\Delta \theta$ and $\Delta \varphi$ represent the bond stretching increment, the bond angle variation and the torsion angle variation, respectively. It is assumed that in a hexagonal graphite sheet, only the atom B undergoes a micro linear displacement δ in the AB direction, as shown in Fig. 5.3. The internal coordinate of bond DB and CB will also change as $\llcorner DBB^* = 60°$. Therefore,

$$\Delta r = BE = \tfrac{1}{2}*\delta \tag{5.5}$$

$$\delta\perp = EB^* = (\sqrt{3})/2\delta \tag{5.6}$$

as δ is micro ,so $\Delta\theta \approx (\delta\perp / L) = [\sqrt{3}(\delta) /(2L)]$

Fig 5.3 Displacements of atoms in graphite sheet and change in internal coordinates in BD

According to the theory of the Tersoff-Brenner force field, the change of the total steric potential energy can be determined as follows:

$$U_r = \frac{1}{2}K_r(\Delta r_{AB})^2 + \frac{1}{2}K_r(\Delta r_{BD})^2 + \frac{1}{2}K_r(\Delta r_{BC})^2 \tag{5.7}$$

$$U_\theta = \frac{1}{2}K_\theta(\Delta\theta_{\angle ABC}) + \frac{1}{2}K_\theta(\Delta\theta_{\angle ABD}) + \frac{1}{2}K_\theta(\Delta\theta_{\angle BDF}) + \frac{1}{2}K_\theta(\Delta\theta_{\angle BCG})$$

$$+ \frac{1}{2}K_\theta(\Delta\theta_{\angle BCH}) + \frac{1}{2}K_\theta(\Delta\theta_{\angle DBC}) + \frac{1}{2}K_\theta(\Delta\theta_{\angle BDI})$$

$$= \frac{1}{2}K_\theta(\Delta\theta)^2 \times 6 + \frac{1}{2}K_\theta(\Delta\theta \times 2)^2 = (15\delta^2 / 4L^2)K_\theta \tag{5.8}$$

From the viewpoint of the theory of continuum mechanics, because the chemical properties of C-C bonds in the graphite sheets are identical, it can be assumed that the graphite sheet can be treated as a plane frame-like structure, the C-C bonds as uniform beam models. Moreover, suppose that the sections of beams are uniformly round and the

carbon atoms act as joints of the related load-bearing beam models. So the analysis above can be considered as showing that beam AB undergoes a micro displacement δ under axial force, with the other joints fixed. The axial displacement Δl and the deflection w of beam DB and beam CB may be calculated, and

$$\Delta l = -\Delta r = -(\tfrac{1}{2})\,\delta \quad, \quad w = \delta\perp = (\sqrt{3})/2\delta \tag{5.9}$$

As stated above that δ is micro, the deformation of the structure obeys the linear elastic-continuum theory, the changes of total strain energies of this plane frame structure under the action of the axial force N and bending moment M as shown in Fig 5.4 can be written as

$$U = U_A + U_M \tag{5.10}$$

where

$$U_A = \sum_{i=1}^{3}\frac{1}{2}\int_0^L \left(\frac{N_i^2}{EA}\right)dx = \frac{EA}{2L}\delta^2 + \frac{EA}{2L}\left(\frac{\delta}{2}\right)^2 \times 2$$

$$U_M = \sum_{i=1}^{3}\frac{1}{2}\int_0^L \left(\frac{M_i^2}{EI}\right)dx = \int_0^L \frac{\left(\frac{12EI}{L^3}\frac{\sqrt{3}}{2}\delta x - \frac{6EI}{L^2}\frac{\sqrt{3}}{2}\delta\right)^2}{EI}dx = \frac{9EI}{L^3}\delta^2 \tag{5.11}$$

$$U_T = \sum_{i=1}^{3}\frac{1}{2}\int_0^L \frac{T_i^2}{GJ}dx = \sum_{i=1}^{3}\frac{GJ}{2L}\left(\Delta\varphi_i\right)^2$$

$$U_M = \sum_{i=1}^{3}\frac{1}{2}\int_0^L \left(\frac{M_i^2}{EI}\right)dx = \int_0^L \frac{\left(\frac{12EI}{L^3}\frac{\sqrt{3}}{2}\delta x - \frac{6EI}{L^2}\frac{\sqrt{3}}{2}\delta\right)^2}{EI}dx = \frac{9EI}{L^3}\delta^2 \tag{5.12}$$

The beams will twist in space frame structures and the strain energy of uniform beams under the action of the pure torsion T is

$$U_T = \sum_{i=1}^{3} \frac{1}{2} \int_0^L \frac{T_i^2}{GJ} dx = \sum_{i=1}^{3} \frac{GJ}{2L} \left(\Delta \varphi_i \right)^2 \tag{5.13}$$

where $\Delta\varphi_i$ is the relative rotation between the two ends of the ith beam and is equivalent to the angle variation of the i-th bond twisting.
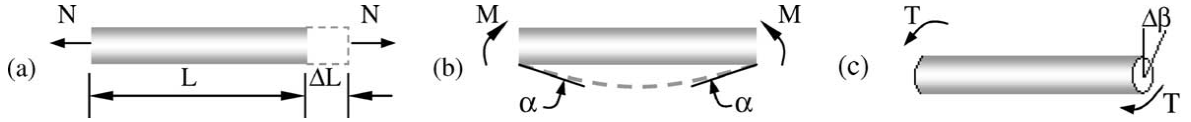

Fig 5.4 Pure tension, bending and torsion of an element [22]

It is evident that both Ur and U_A represent the stretching energy, both U_θ and U_M represent the bending energy, and both Uτ and U_T represent the torsional energy. So it can be $U_A = U_R$, $U_M = U_\theta$ and $U_T = U\tau$. Thus by comparing Eq.(5.11) with Eq.(5.7), Eq.(5.12) with Eq.(5.8), and Eq.(5.13) with Eq.(5.4), the following equations can be obtained.

$$\frac{EA}{L} = K_r \tag{5.14}$$

$$\frac{EI}{L} = \frac{5}{12} K_\theta \tag{5.15}$$

$$\frac{GJ}{L} = K_\tau \tag{5.16}$$

From equations (5.14)-(5.16), the sectional stiffness parameters of beam models are determined and the linkage between the nano-scale mechanics and the continuum mechanics is established. Then, based on the theory of continuum mechanics, the material

mechanical properties of graphite sheets and carbon SWNTs can be obtained by numerical simulative calculation.

By assuming a circular beam section with diameter d, and setting $A=\pi d^2/4$, $I=\pi d^4/64$ and $J=\pi d^4/32$ we get,

$$d = 4\sqrt{\frac{k_\theta}{k_r}}, E = \frac{k_r^2 L}{4\pi k_\theta}, G = \frac{k_r^2 k_\tau L}{8\pi k_\theta^2} \tag{5.17}$$

For, $k_r = 6.52 \times 10^{-7}$ N nm^{-1}, $k_\theta = 8.76 \times 10^{-10}$ N nm rad^{-2},

$k_\tau = 2.78 \times 10^{-10}$ N nm rad^{-2} and $L=a_{c-c}=0.1421$ nm,

We get, d=0.147nm, E=5.49 TPa , G = 0.871 TPa.

5.1.4 Calculation of Elastic Moduli

The Young's modulus of a material is the ratio of normal stress to normal strain as obtained from a uniaxial tension test. Following this definition, the Young's modulus of SWCNTs is been calculated using the following equation

$$Y = \frac{(F / A_0)}{(\Delta H / H_0)} \tag{5.18}$$

where, $A_0 = \pi Dt$ and *Ho* is initial length. where *F* is the total applied force, A_0, the cross-sectional area, H_0 the initial length and ΔH the elongation. A_0 is equal to πDt where D is the mean diameter of the tube as seen in Fig.5.5. In the case of armchair and zigzag SWCNTs, their initial length H_0 is preset since all the sub marginal nodes are situated at the same plane. However, in case of chiral SWCNTs, the sub marginal nodes are not at the same plane and therefore, H_0 is taken as the average of the longitudinal coordinates of the

sub marginal nodes. ΔH is taken in all cases as the average of the displacements of the sub marginal nodes. For calculating the Shear modulus of SWCNTs, the following relation is used
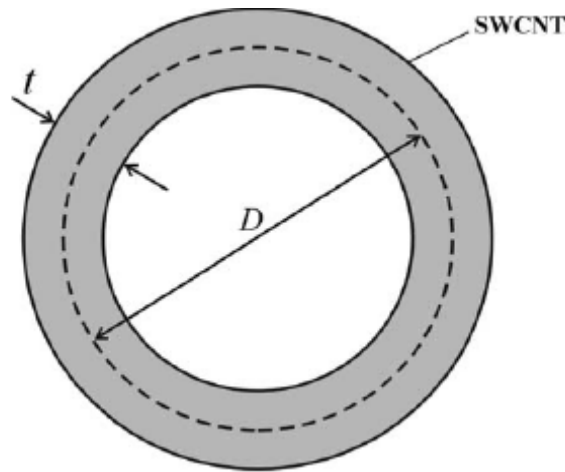
$$S = \frac{TH_0}{\theta J_0} \qquad (5.19)$$

Fig 5.5 Schematic of the cross-section of a SWCNT.

where T stands for the torque acting at the one end of the SWCNT, θ for the torsional angle of the tube and J_0 for the polar moment of inertia of the cross-sectional area. For calculating J_0, the SWCNT is considered as a hollow tube of diameter D and thickness t. In this case, J_0 is equal to

$$J_0 = \left(\frac{\pi}{32}\right)\left[(D+t)^4 - (D-t)^4\right] \qquad (5.20)$$

The elongation ΔH and the torsional angle θ are calculated by the FE model. In order to apply the conditions of tension and torsion, the nodes of the bottom end of the SWCNT have been fully bult-in (zero displacement and rotation conditions), while the nodes of the

upper end, are subjected to tensile and tangential forces, respectively. Fig.5.6A and 5.6B shows the FE meshes of the SWCNTs with the applied boundary conditions. The first and third SWCNT have been subjected to tension, while the second SWCNT to torsion. As may be seen in Fig.5.6B, in the case of torsion loading, the nodes of the upper end are restricted from moving in the radial direction. In order to apply the boundary conditions of tension and torsion, the nodes of the bottom end of the SWCNT have been fully built-in (zero displacement and rotation conditions), while the nodes of the upper end, are subjected to tensile and tangential forces, respectively.

5.1.5 Calculation of Coefficient of Thermal Expansion (CTE)

Here graphene sheets and SWCNTs are modeled using ANSYS commercial FE code. The uniform temperature is applied to each node by fixing the nodes at one end (zero displacement). The coefficient of thermal expansion of the CNTs in the axial direction is given by

$$\alpha_{axial} = \frac{1}{H_0} \frac{\Delta H}{\Delta T_t}$$
(5.21)

where, ΔH is the change in length of the nanotube, H_0 is the length of the carbon nanotube and ΔT_t is the change in temperature. Similarly, the coefficient of thermal expansion of the CNTs in the radial direction is given by

$$\alpha_{radial} = \frac{1}{R} \frac{\Delta R}{\Delta T_t}$$
(5.22)

where, R is the radius of the CNT and ΔR is the change in radius of the nanotube. The coefficient of linear thermal expansion of carbon bond as 0.0000019 cm/cm/˚C is adopted based on the earlier reference.
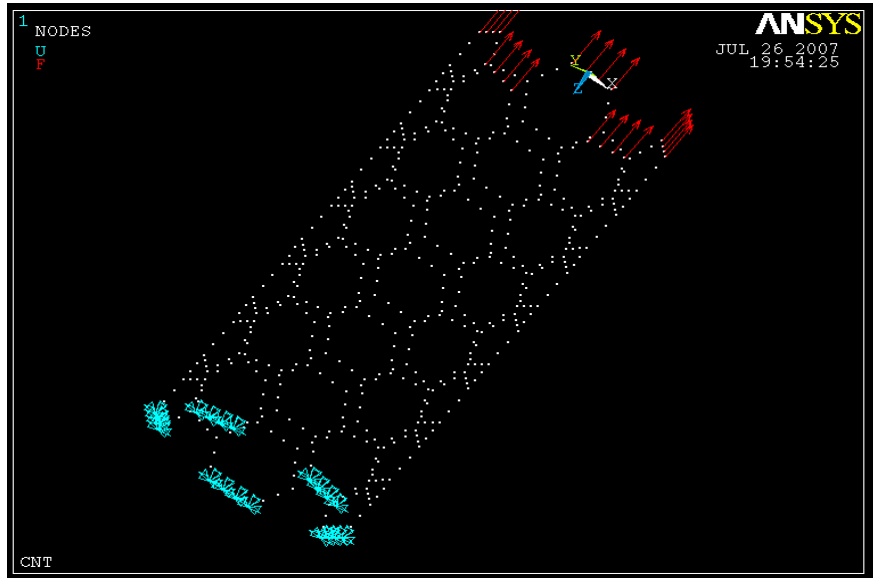

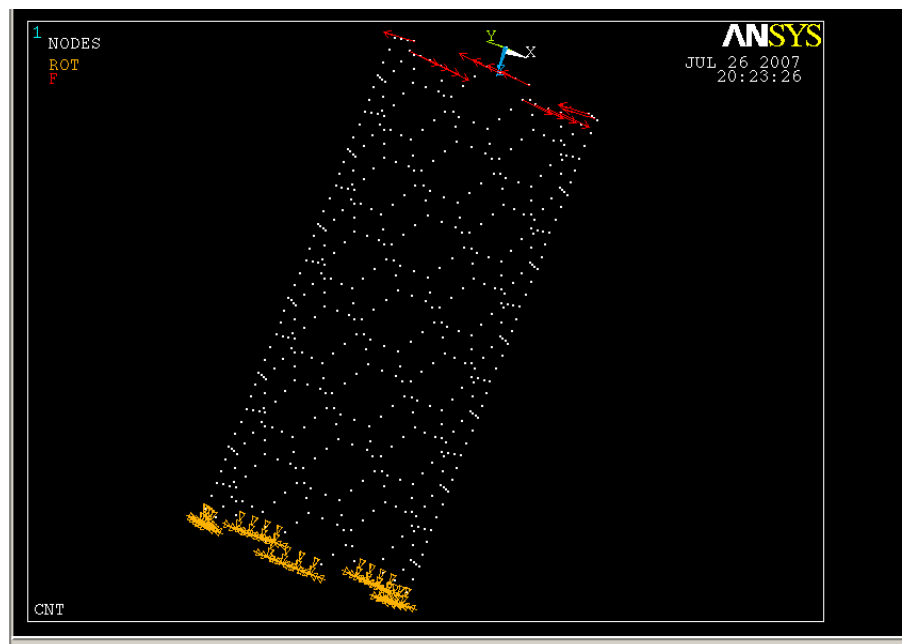**Fig 5.6A FE nodal diagram of (5,5) SWCNT under tensile load**

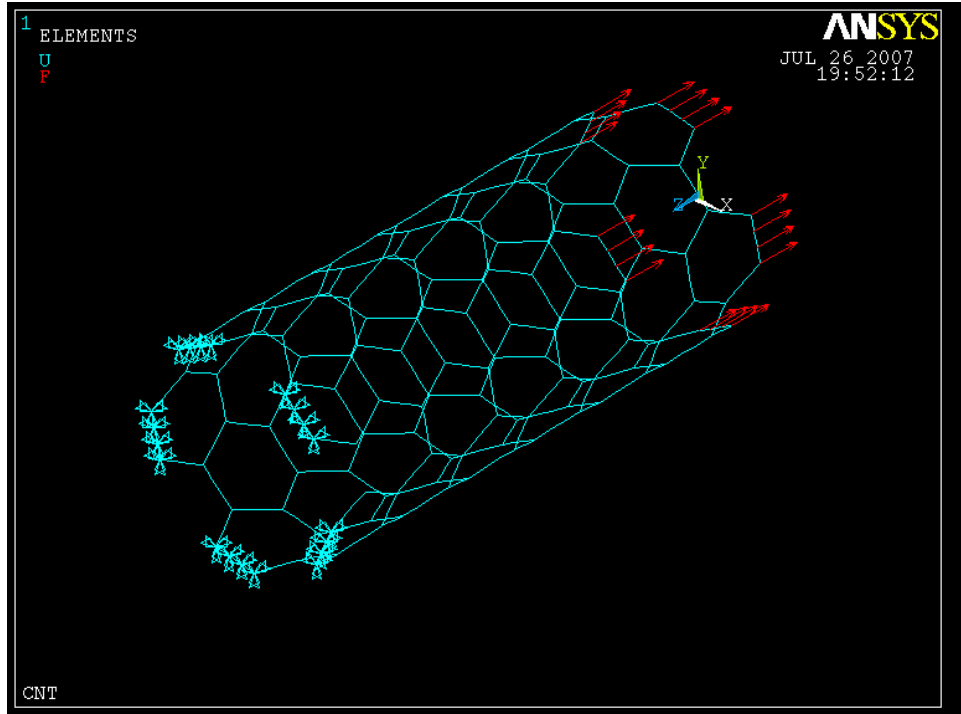**Fig 5.6B FE nodal diagram of (5,5) SWCNT under torsional load**

Fig 5.6C FE mesh of (5,5) SWCNT under tensile load

Table 5.1 Beam element properties I

Cross sectional area, A:	0.0169785 nm^2
Moments of Inertia, I1,I2:	$2.293\text{E-}5 \text{ nm}^4$
Torsional constant, J:	0.0376735 nm^4

Table 5.2 Nanotube geometric and mesh properties

Type:	Armchair
Chirality:	5,5
Avg. Diameter:	0.677901 nm
Length:	1.5987 nm
Number of nodes:	140
Number of elements:	600
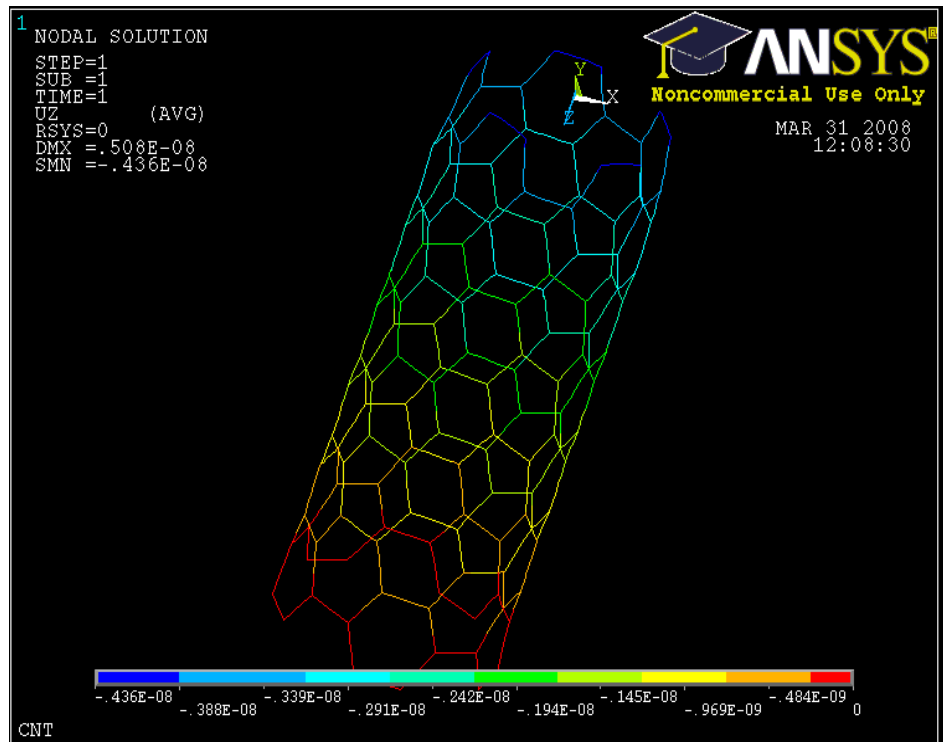
Fig 5.7 Displacement solution of (5,5) nanotube

5.1.6 Results and Discussions

The data in Table 5.1 & 5.2 is given as input of Ansys and the elongation ΔH and the torsional angle θ are calculated by the FE model as shown in the Fig 5.7. Varying the wall thickness we analyze the variation of young's modulus. Varying the diameter of CNT, we analyze the variation in elastic moduli and thermal coefficient of linear expansion in axial and radial directions.
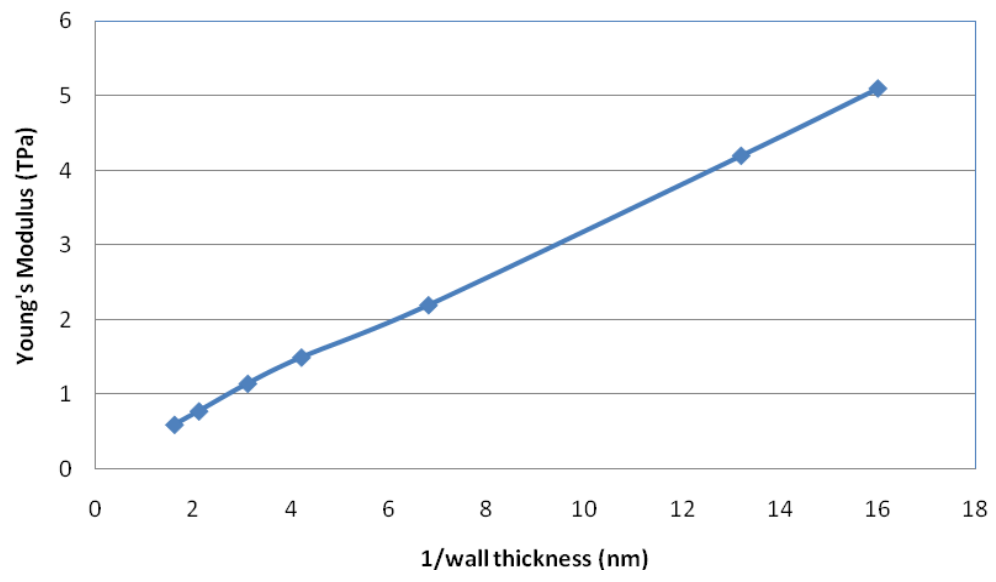
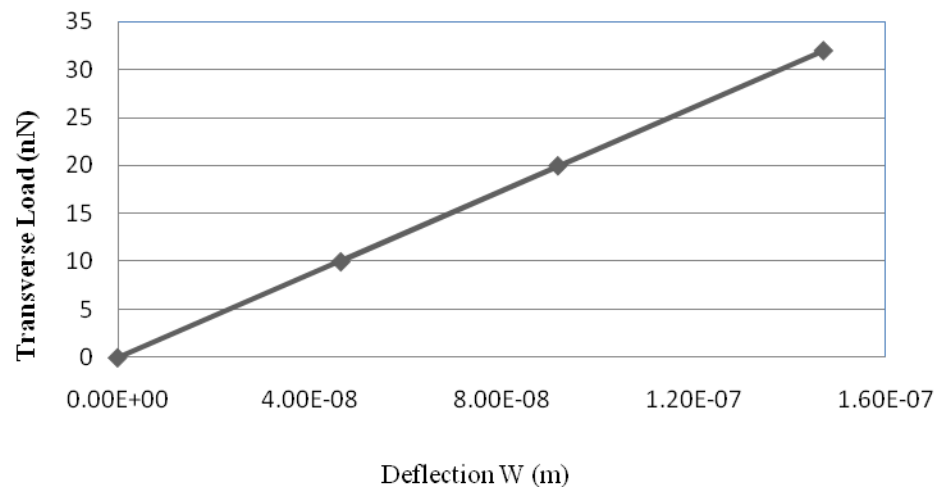**Fig 5.8 Variation of Young's modulus with wall thickness for (5,5) armchair nanotube**

Fig.5.9 Nanotube bending behavior

Hence, we observe that the young's modulus increases linearly with 1/wall thickness in Fig 5.8 and force-deflection relationship is also linear in Fig 5.9.
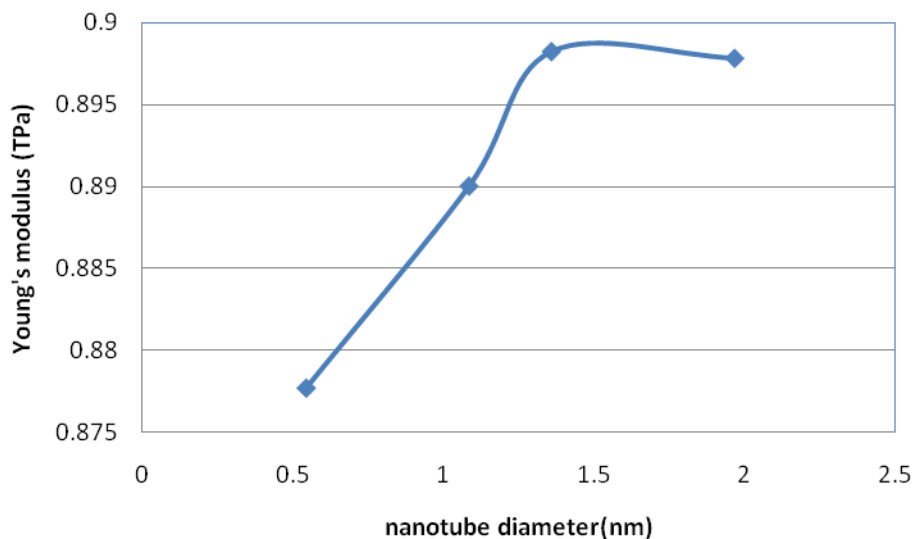
Fig 5.10 Variation of Young's modulus of armchair SWCNTs (for t=0.34 nm) with nanotube diameter
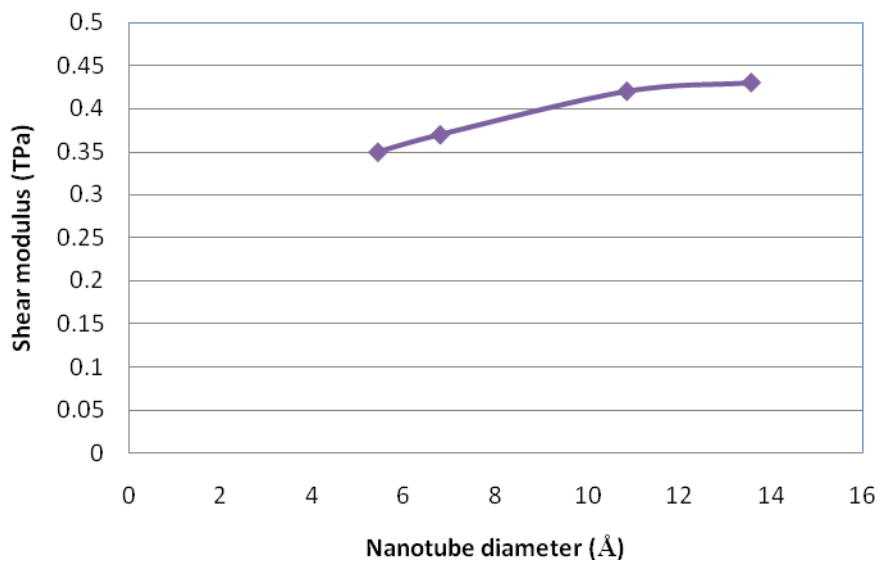

Fig 5.11 Variation of Shear modulus of SWCNTs with nanotube diameter

Hence in Fig 5.10 & Fig 5.11, we observe that both E and G increase with increase in tube diameter and reach a constant value for diameters more than 1.5 nm or 15 Å.
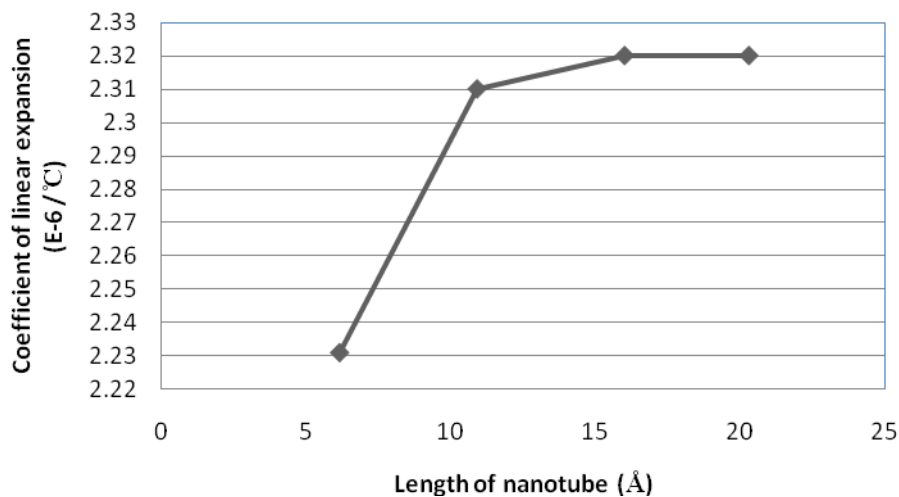
Fig 5.12 Variation of Coefficient of linear expansion with nanotube length

We observe from Fig 5.12 that the thermal coefficient of linear expansion of nanotube increases with nanotube length and reaches a constant value of 2.32E-6 / ^{0}C for nanotubes of length 17 Å or greater.

The plots below in Fig 5.13 & Fig 5.14 depict that the similar variation is seen for α_{axial} and α_{radial} with increase in tube diameter. α_{axial} reaches a value of 2.32E^{-6} / ^{0}C and α_{radial} reaches a constant value of 2.13E^{-6} / ^{0}C.
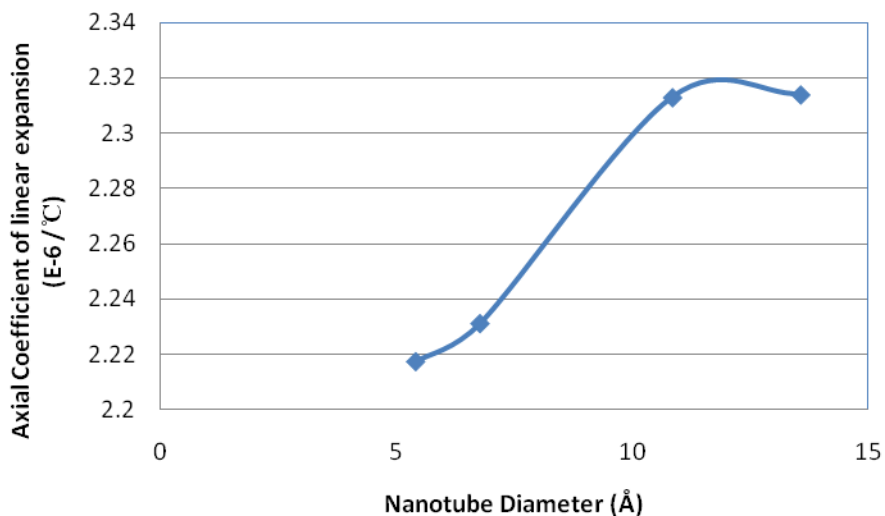
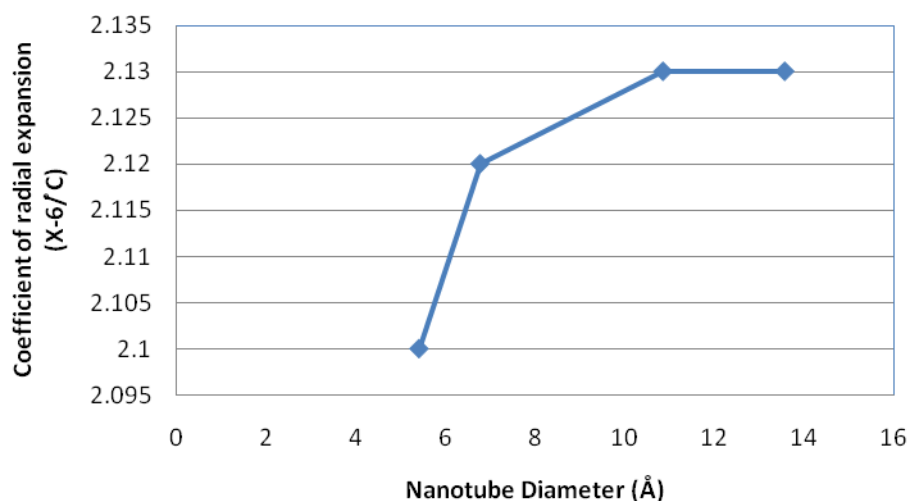**Fig 5.13 Variation of Axial Coefficient of linear expansion with nanotube diameter**

Fig 5.14 Variation of Radial Coefficient of linear expansion with nanotube diameter

5.2 Finite Element Modeling of Double Walled Carbon Nanotube

Until now we have observed the behavior of SWNT by bending, stretching and twisting them and also subjecting them to elevated temperatures. In an attempt to understand the behavior of multi walled nanotubes, in this section we will study the

behavior of DWNT under tensile load. The challenge involved in modeling a DWNT is to account for the van der Waal's forces between the adjacent layers.

The forces are simulated by truss rods between nodes of adjacent layers as seen in Fig 5.15. The individual nanotubes are modeled as usual using 3D elastic beam elements. In this model, based on the Lennard-Jones ''6–12'' potential, the van der Waals force between interacting atoms is written as

$$F(r) = -\frac{dU(r)}{dr} = 24\frac{\varepsilon}{r}\left[2\left(\frac{\sigma}{r}\right)^{13} - \left(\frac{\sigma}{r}\right)^{7}\right]$$

(5.23)

Where r is the inter-atomic distance, ε and σ are the Lennard-Jones parameters. For carbon atoms, the Lennard-Jones parameters are $\varepsilon = 0.0556$ kcal/mole and $\sigma = 3.4$Å.
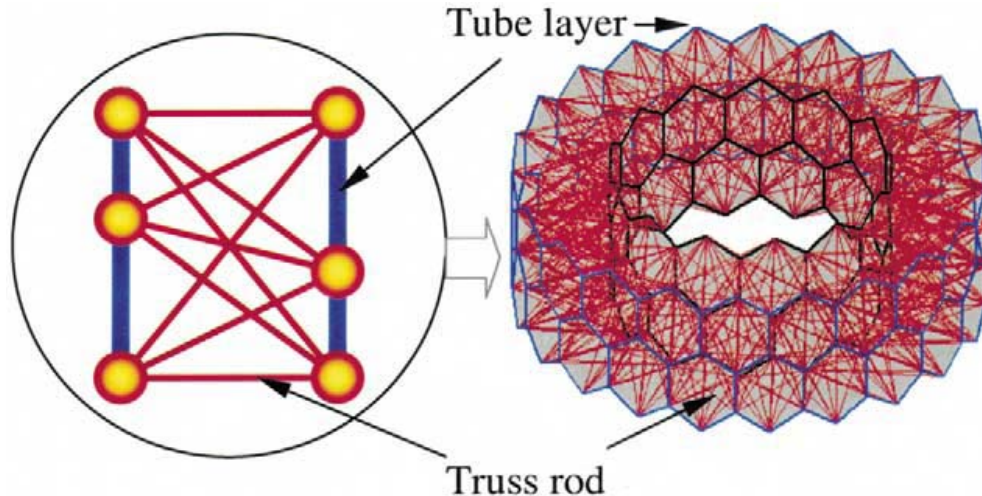

Fig 5.15 Truss rods for simulating van der waals forces [23]

Based on the criterion that the van der Waals force from the lennard Jones Potential is negligible when the distance between atoms is beyond 2.5σ, a truss rod is activated

whenever the distance between located in neighboring tube layers is less than 2.5 σ. The young's modulus is then expressed as

$$Y = \frac{(F / A_0)}{(\Delta H / H_0)} \tag{5.24}$$

where, F is the total force acting on the atoms at one end of the nanotube, $A_0 = \left(\dfrac{\pi}{4}\right)\left[\left(D_0 + 3.4\right)^2 - \left(D_i - 3.4\right)^2\right] Å^2$ represents the cross sectional area of the multi walled tube with D_o and D_i as the outer and inner tube diameters and H_o is the initial length of the tube and ΔH is the elongation of the tube.
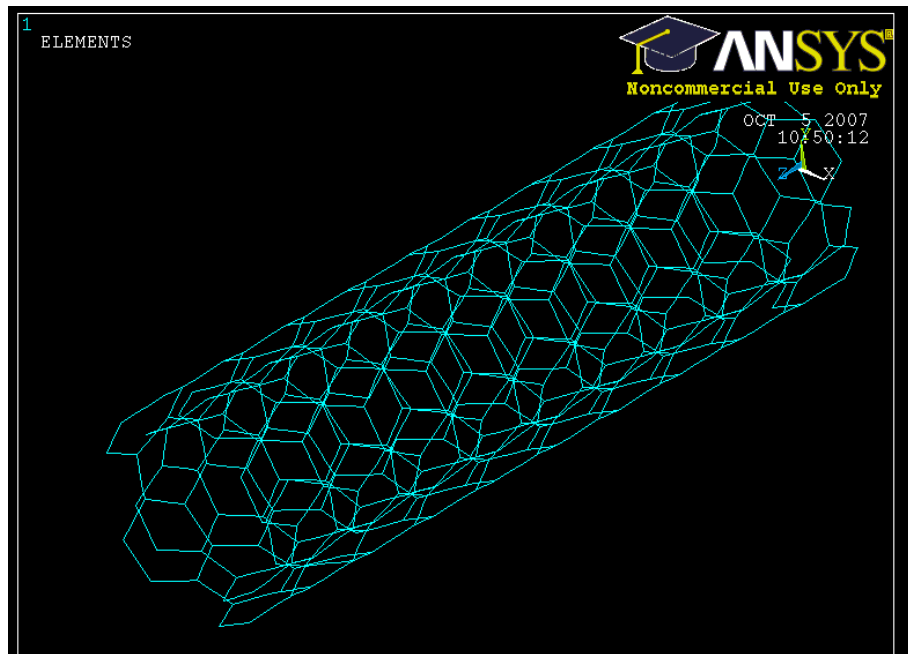
* For the above specimen, the no. of van der Waal's truss rods are 16,662.

Fig 5.16 3D Elastic beam element mesh of DWNT

Table 5.3 Beam element properties II

Cross sectional area, A	0.0169785 nm^2
Moments of Inertia, I_1, I_2:	2.293E-5 nm^4
Torsional constant, J	0.0376735 nm^4

Table 5.4 Inner SWNT geometric and mesh properties

Type	Armchair
Chirality	4,4
Avg. Diameter	0.54233 nm
Length	2.3366 nm
Number of nodes	160
Number of elements	732

Table 5.5 Outer SWNT geometric and mesh properties

Type	Armchair
Chirality	8,8
Avg. Diameter	1.085 nm
Length	2.3365 nm
Number of nodes	321
Number of elements	1304

Since the van der Waal's force is non linearly varying with length of the truss rod, it was possible to analyze only small length nanotubes using ANSYS by giving the data in tables 5.3, 5.4 and 5.5 as input. So, a FORTRAN code has been written for modeling the nanotubes using 3D beam elements discussed in chapter 4 and the van der Waal's forces using truss elements. Then using the connectivity and the calculated forces fed as nodal boundary conditions in ANSYS, the elongation of the DWNT has been calculated for few specimens with small lengths of 0.7-1 nm as shown in Fig 5.17.

The major difficulty involved in FE coding of nanotubes include conversion of element coordinates from local coordinate to global coordinate system (using the 3D

transformation matrices for rotation and translation) for assembling the elemental equations to solve the total system of equations and get the global displacements. Also, the boundary conditions at the end nodes need to be carefully applied. If this can be implanted, then we are well equipped to analyze longer tubes as shown in Fig 5.16 and get more accurate values for elastic moduli of MWNTs.
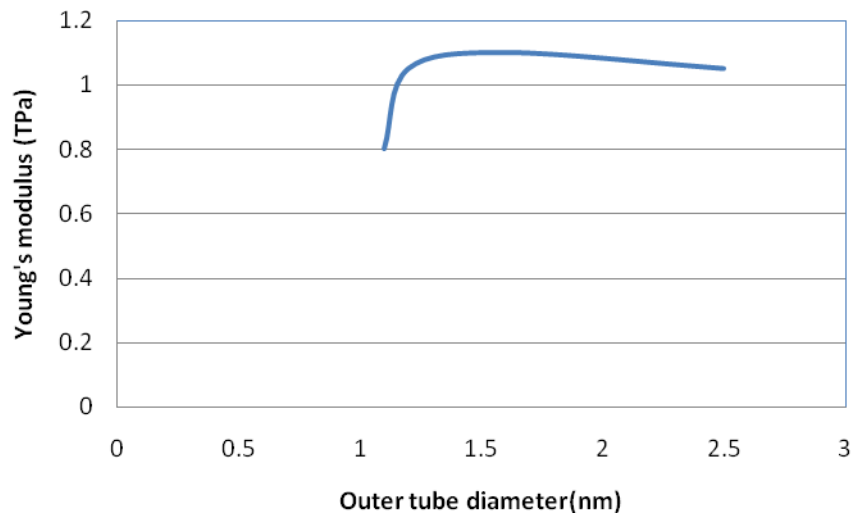

Fig 5.17 Variation of Young's modulus with outer tube diameter for armchair DWNT

Regarding the experimental results of Young's moduli of MWCNTs, Wong et al. [24] and Salvetat et al. [25] reported values of 1.28 ±0.59 and 0.81±0.41 TPa, respectively, using AFM-based experiments. These data are comparable to the present prediction of 1.05±0.05 TPa.

The FE code can be extended to model and study the properties of nano-composites. Multi-scale modeling of compressive behavior of carbon nanotube/ polymer composites can be done on similar lines where the nanotube is modeled at the atomistic

scale by the molecular structural mechanics method, and the matrix deformation is analyzed at the macroscopic scale by the continuum finite element method. The nanotube and polymer matrix are assumed to be bonded by van der Waal's interactions at the interface as shown in Fig 5.18.

The stress distributions at the nanotube/ polymer interface under isostrain and isostress loading conditions have to be examined to study the load transfer between nanotubes and matrix. Under compressive loading, one of the failure modes of a structural component is elastic instability, namely, buckling. For understanding the performance of nanotube/polymer composites under compression, elastic buckling is a fundamental issue that needs to be addressed. According to the theory of structural stability, the buckling force of a structural element can be determined by the eigen-value analysis, which requires the consideration of the geometrically nonlinear problem since For the nanotube/ polymer interface, the force–displacement relationship of a truss rod is nonlinear.

5.2.1 Modeling of Polymer Matrix

Two kinds of three dimensional finite elements are used in the meshing of the matrix [38]: 20-node iso-parametric cubic element (Solid 95 in ANSYS) and 15-node iso-parametric wedge-shaped element (Solid 147/186). The 20-node element is used in the circumferential region surrounding the nanotube, whereas the 15-node element is used in the regions directly above and below the nanotube as shown in Fig 5.19 & Fig 5.20.
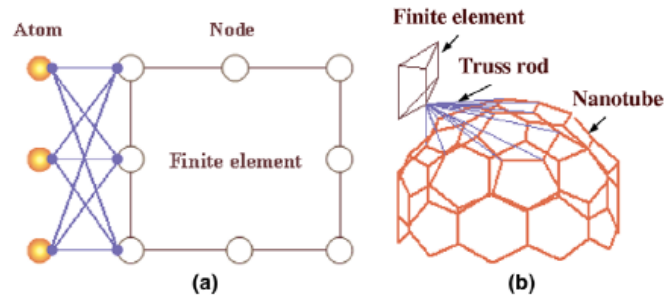
Fig 5.18 Illustrations of truss rods connecting nodes in finite elements with carbon atoms: (a) on the nanotube lateral surface and (b) on the nanotube end cap region [38]
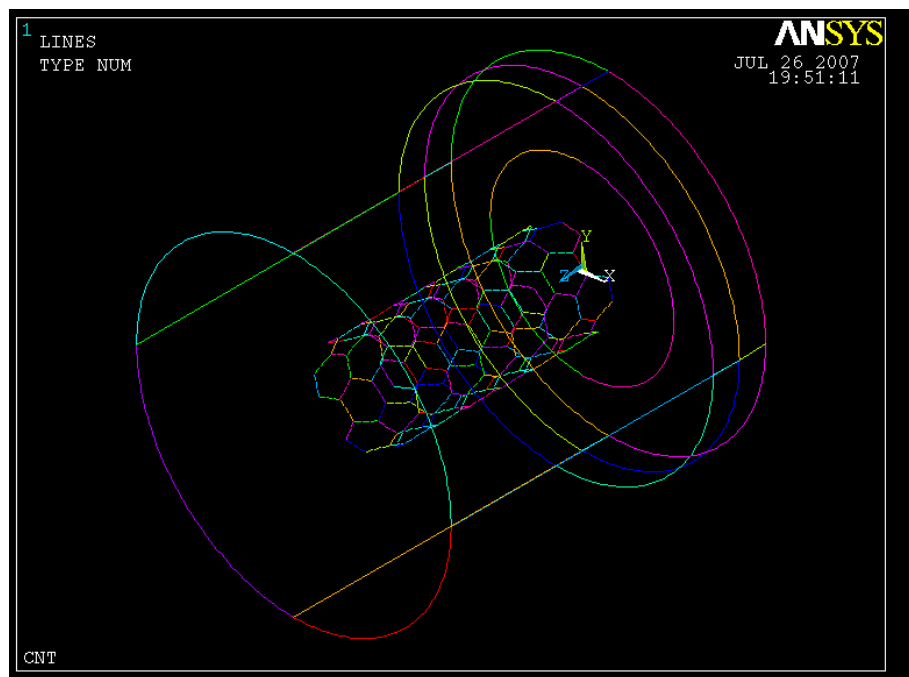

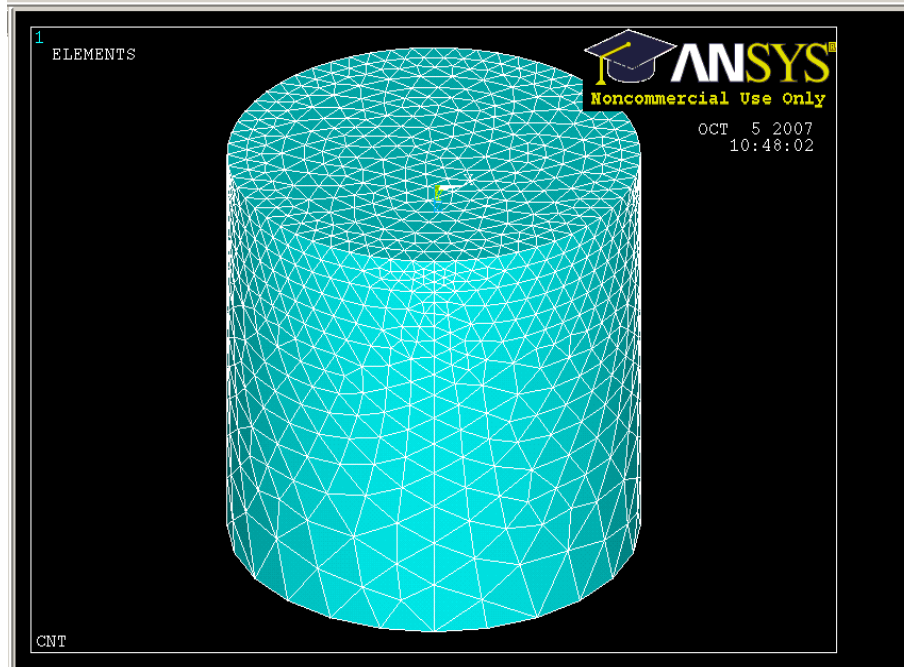**Fig 5.19 Computational model for nanotube/polymer composites**

Fig 5.20 Mesh of polymer composite matrix

Then, following the procedure of the structural mechanics technique as in the previous models of SWNT and DWNT, the nanotube deformation under certain loading conditions can be readily solved.

CHAPTER VI

MOLECULAR DYNAMIC SIMULATIONS OF CARBON NANOTUBES/ POLYMER

COMPOSITES

Molecular mechanics and molecular dynamics simulations promotes science-based understanding of the properties of complex materials and phenomena. In the development of carbon nanotube/ polymer composites, they offer insight into the local interactions among individual atoms based on the discrete models of the nanotubes and polymer matrix. They have provided enough detailed information for understanding the load transfer and mechanical behavior of carbon nanotube/ polymer composites. However, these simulations are currently limited to very small length and time scales and therefore are not suitable for large-scale analysis in real-life applications. Regarding the modeling of carbon nanotube/ polymer composites, it is required to incorporate more structural characteristics of carbon nanotubes into the computational models, such as structural defects on the nanotube surface, ropes or bundles of nanotubes, and waviness of the nanotubes in the nano-composites.

6.1 Introduction to Molecular Dynamics Simulation

In this chapter a summary is given of the key ingredients necessary to carry out a molecular dynamics simulation, with particular emphasis on macromolecular systems. We discuss the form of the intermolecular potential for molecules composed of atoms, and of non-spherical sub-units, giving examples of how to compute the forces and torques. We also describe some of the MD algorithms in current use. Finally, we briefly

refer to the factors that influence the size of systems, and length of runs, that are needed to calculate statistical properties.

6.1.1   The Aims of Molecular Dynamics

Computer simulations are carried out in the hope of understanding the properties of assemblies of molecules in terms of their structure and the microscopic interactions between them. This serves as a complement to conventional experiments, enabling us to learn something new, something that cannot be found out in other ways. The two main families of simulation technique are molecular dynamics (MD) and Monte Carlo (MC); addition ally, there is a whole range of hybrid techniques which combine features from both. In this lecture we shall concentrate on MD. The obvious advantage of MD over MC is that it gives a route to dynamical properties of the system: transport coefficients, time-dependent responses to perturbations, rheological properties and spectra.

Computer simulations act as a bridge between microscopic length and time scales and the macroscopic world of the laboratory: we provide a guess at the interactions between molecules, and obtain 'exact' predictions of bulk properties. The predictions are 'exact' in the sense that they can be made as accurate as we like, subject to the limitations imposed by our computer budget. At the same time, the hidden detail behind bulk measurements can be revealed. An example is the link between the diffusion coefficient and velocity autocorrelation function (the former easy to measure experimentally, the latter much harder). Simulations act as a bridge in another sense: between theory and experiment.

6.2   Molecular Interactions

Molecular dynamics simulation consists of the numerical, step-by-step, solution of the classical equations of motion, which for a simple atomic system may be written

$$m_i \ddot{r}_i = f_i \qquad f_i = \frac{\partial}{\partial \ddot{r}_i} u \qquad (6.1)$$

For this purpose we need to be able to calculate the forces f_i acting on the atoms, and these are usually derived from a potential energy $U(r^N)$, where $r^N = \left(r^1, r^2, r^3 \ldots \ldots r^N \right)$ represents the complete set of 3N atomic coordinates. In this section, we focus on this function $U(r^N)$, restricting ourselves to an atomic description for simplicity.

6.2.1   Non-bonded Interactions

The part of the potential energy $U_{non-bonded}$ representing non-bonded interactions between atoms is traditionally split into 1-body, 2-body, 3-body ... terms:

$$u_{non-bonded}(r^N) = \sum_i u(r_i) + \sum_i \sum_{j>i} v(r_i, r_j) + \ldots. \qquad (6.2)$$

The $u(r)$ term represents an externally applied potential field or the effects of the container walls; it is usually dropped for fully periodic simulations of bulk systems. Also, it is usual to concentrate on the pair potential $v(\mathbf{r_i}, \mathbf{r_j}) = v(\mathbf{r_{ij}})$ and neglect three-body (and higher order) interactions. There is an extensive literature on the way these potentials are determined experimentally, or modeled theoretically. The Lennard-Jones potential is the most commonly used form:

$$U^{LJ}(r) = 4\varepsilon\left[\left(\frac{\sigma}{r}\right)^{12} - \left(\frac{\sigma}{r}\right)^{6}\right]$$

(6.3)

This potential was used, for instance, in the earliest studies of the properties of liquid argon. For applications in which attractive interactions are of less concern than the excluded volume effects which dictate molecular packing, the potential may be truncated at the position of its minimum, and shifted upwards to give what is usually termed the WCA model. If electrostatic charges are present, we add the appropriate Coulomb potentials

$$U^{coulomb}(r) = \frac{Q_1 Q_2}{4\Pi\varepsilon_0 r},$$

(6.4)

where Q_1, Q_2 are the charges and ε_0 is the permittivity of free space.

6.2.2 Bonding Potentials

For molecular systems, we simply build the molecules out of site-site potentials of the form of Eq. (6.3) or similar. Typically, a single-molecule quantum-chemical calculation may be used to estimate the electron density throughout the molecule, which may then be modeled by a distribution of partial charges via Eq. (6.4), or more accurately by a distribution of electrostatic multipoles. For molecules we must also consider the intra-molecular bonding interactions. The simplest molecular model will include terms of the following kind:

$$U_{\text{int}ramolecular} = \frac{1}{2}\sum_{bonds} k_{ij}^{r}(r_{ij} - r_{eq})^2$$

(6.5a)

$$+\frac{1}{2}\sum_{\substack{bend \\ angles}} k_{ijk}^{\theta}(\theta_{ijk}-\theta_{eq})^2 \tag{6.5b}$$

$$+\frac{1}{2}\sum_{\substack{torsion \\ angles}}\sum_{m} k_{ijkl}^{\phi,m}(1+\cos(m\phi_{ijkl}-\gamma_m)) \tag{6.5c}$$

The "bonds" will typically involve the separation $r_{ij}=|r_i-r_j|$ between adjacent pairs of atoms in a molecular framework, and we assume in Eq. (6.5a) a harmonic form with specified equilibrium separation, although this is not the only possibility. As seen in Fig 6.1, the "bend angles" θ_{ijk} are between successive bond vectors such as r_i-r_j and r_j-r_k, and therefore involve three atom coordinates:
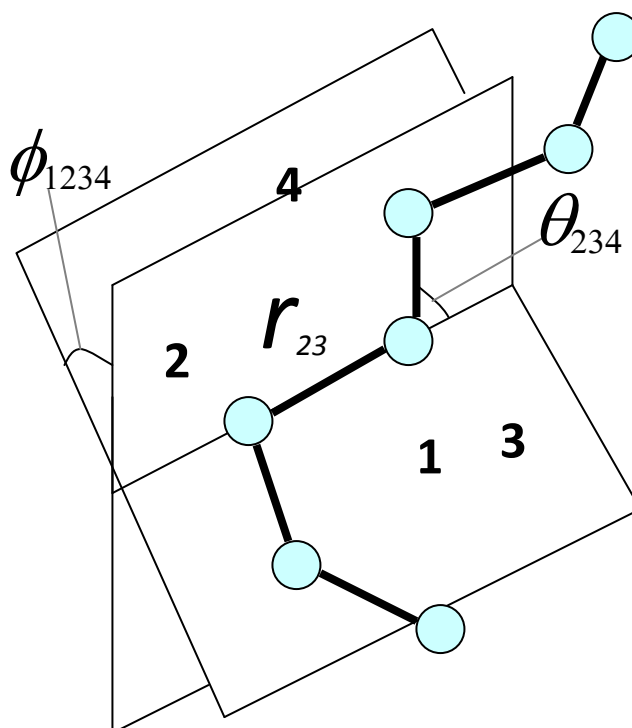

Fig 6.1 Geometry of a simple chain molecule, illustrating the definition of interatomic distance r_{23}, bend angle θ_{234}, and torsion angle ϕ_{1234}

$$\cos\theta_{ijk} = \hat{r}_{ij}.\hat{r}_{ij} = (r_{ij}.r_{ij})^{-\frac{1}{2}}(r_{jk}.r_{jk})^{-\frac{1}{2}}(r_{ij}.r_{jk})$$

(6.6)

where $\hat{r} = r/r$. Usually this bending is taken to be quadratic in the angular displacement from the equilibrium value, as in Eq. (6.5b), although periodic functions are also used. The "torsion angles" ϕ_{ijk} are defined in terms of three connected bonds, hence four atomic coordinates:

$$cos\phi_{ijkl} = -\hat{n}_{ijk} \bullet \hat{n}_{jkl} \qquad where, \qquad n_{ijk} = r_{ij} \times r_{jk}, \ n_{jkl} = r_{jk} \times r_{kl}$$

(6.7)

torsional potential involves an expansion in periodic functions of order m $= 1, 2, .,$ Eq. (6.5c).

6.3 Force Calculation

Having specified the potential energy function $U(r^N)$, the next step is to calculate the atomic forces

$$f_i = -\frac{\partial}{\partial r_i}U(r^N)$$

(6.8)

For site-site potentials this is a simple exercise. For the intra-molecular part of the potential, it is a little more involved, but still a relatively straightforward application of the chain rule.

6.4 The MD Algorithm

A system composed of atoms with coordinates $r^N = (r_1, r_2, ...r_N)$ and potential energy $U(r^N)$, we introduce the atomic momenta $p^N = (p_1, p_2, ...p_N)$, in terms of

which the kinetic energy may be written $K(\mathbf{p}^N) = \sum_{i=1}^{N} |\mathbf{p}_i|^2 / 2m_i$. Then the energy, or hamiltonian, may be written as a sum of kinetic and potential terms $H = K + U$. Write the classical equations of motion as

$$\dot{\mathbf{r}}_i = \mathbf{p}_i / m_i \quad \text{and} \quad \dot{\mathbf{p}}_i = \mathbf{f}_i \tag{6.9}$$

This is a system of coupled ordinary differential equations. Many methods exist to perform step-by-step numerical integration of them. Characteristics of these equations are: (a) they are 'stiff', i.e. there may be short and long timescales, and the algorithm must cope with both; (b) calculating the forces is expensive, typically involving a sum over pairs of atoms, and should be performed as infrequently as possible. Also we must bear in mind that the advancement of the coordinates of two functions: (i) accurate calculation of dynamical properties, especially over times as long as typical correlation times τa of properties a of interest (we shall define this later); (ii) accurately staying on the constant-energy hyper-surface, for much longer times $\tau_{run} \gg \tau_a$, in order to sample the correct ensemble.

     To ensure rapid sampling of phase space, we wish to make the timestep as large as possible consistent with these requirements. For these reasons, simulation algorithms have tended to be of *low order* (i.e. they do not involve storing high derivatives of positions, velocities etc.): this allows the time step to be increased as much as possible without jeopardizing energy conservation. It is unrealistic to expect the numerical method to accurately follow the true trajectory for very long times τ_{run}. The 'ergodic' and 'mixing' properties of classical trajectories, i.e. the fact that nearby trajectories diverge from each other exponentially quickly, make this impossible to achieve.

6.5 The Verlet Algorithm

There are various, essentially equivalent, versions of the Verlet algorithm, including the original method and a 'leapfrog' form.

$$p_i(t + \frac{1}{2}\delta t) = p_i(t) + \frac{1}{2}\delta t f_i(\bar{t})$$

(6.10a)

$$r_i(t + \delta t) = r_i(t) + \delta t p_i(t + \frac{1}{2}\delta t)/m_i$$

(6.10b)

$$p_i(t + \delta t) = p_i(t + \frac{1}{2}\delta t) + \frac{1}{2}\delta t f_i(t + \delta t)$$

(6.10c)

After step (6.10b), a force evaluation is carried out, to give $f_i(t + \delta t)$ for step (6.10c).

This scheme advances the coordinates and momenta over a timestep δt. As we shall see shortly there is an interesting theoretical derivation of this version of the algorithm. Important features of the Verlet algorithm are: (a) it is *exactly* time reversible; (b) it is *symplectic* (to be discussed shortly); (c) it is *low* order in time, hence permitting long timesteps; (d) it requires just one (expensive) force evaluation per step; (e) it is easy to program.

6.6 Constraints

It is quite common practice in classical computer simulations not to attempt to represent intra-molecular bonds by terms in the potential energy function, because these bonds have very high vibration frequencies (and arguably should be treated in a quantum mechanical way rather than in the classical approximation). Instead, the bonds are treated as being constrained to have fixed length. In classical mechanics, constraints are introduced through the Lagrangian or Hamiltonian formalisms. Given an algebraic

relation between two atomic coordinates, for example a fixed bond length b between atoms 1 and 2, one may write a constraint equation, plus an equation for the time derivative of the constraint

$$\chi(r_1, r_2) = (r_1 - r_2) \bullet (r_1 - r_2) - b^2 = 0 \qquad (6.11a)$$

$$\dot{\chi}(r_1, r_2) = 2(v_1 - v_2) \bullet (r_1 - r_2) = 0 \qquad (6.11b)$$

In the Lagrangian formulation, the constraint forces acting on the atoms will enter thus:

$$m_i \ddot{r}_i = f_i + \Lambda g_i \qquad (6.12)$$

where Λ is the undetermined multiplier and

$$g_1 = -\frac{\partial \chi}{\partial r_1} = -2(r_1 - r_2), \ g_2 = -\frac{\partial \chi}{\partial r_2} = 2(r_1 - r_2) \qquad (6.13)$$

It is easy to derive an exact expression for the multiplier Λ from the above equations; if several constraints are imposed, a system of equations (one per constraint) is obtained. However, this exact solution is not what we want: in practice, since the equations of motion are only solved approximately, in discrete time steps, the constraints will be increasingly violated as the simulation proceeds. The breakthrough in this area came with the proposal to determine the constraint forces in such a way that the constraints are satisfied exactly at the end of each time step. For the original verlet algorithm, this scheme is called SHAKE. The appropriate version of this scheme for the velocity verlet algorithm is called RATTLE.

6.7 Periodic Boundary Conditions

Small sample size means that, unless surface effects are of particular interest, periodic boundary conditions need to be used. Consider 1000 atoms arranged in a $10 \times 10 \times 10$ cube. Nearly half the atoms are on the outer faces, and these will have a large effect on the measured properties. Even for $10^6 = 100^3$ atoms, the surface atoms amount to 6% of the total, which is still nontrivial. Surrounding the cube with replicas of itself takes care of this problem. Provided the potential range is not too long, we can adopt the *minimum image convention* that each atom interacts with the nearest atom or image in the periodic array

In the course of the simulation, if an atom leaves the basic simulation box, attention can be switched to the incoming image as shown in Fig 6.2. Of course, it is important to bear in mind the imposed artificial periodicity when considering properties which are influenced by long-range correlations. Special attention must be paid to the case where the potential range is not short: for example for charged and dipolar systems.

6.8   Neighbour Lists

Computing the non-bonded contribution to the inter-atomic forces in an MD simulation involves, in principle, a large number of pair-wise calculations: we consider each atom i and loop over all other atoms j to calculate the minimum image separations r_{ij}. Let us assume that the interaction potentials are of short range, $v(r_{ij}) = 0$ if $r_{ij} > r_{cut}$, the potential cutoff. In this case, the program skips the force calculation, avoiding expensive calculations, and considers the next candidate j. Nonetheless, the time to

examine all pair separations is proportional to the number of distinct pairs, $1/2 \ N(N-1)$ in an N-atom system, and for every pair one must compute at least r_{ij}^2 ; this still consumes a lot of time.

Some economies result from the use of lists of nearby pairs of atoms. Verlet suggested such a technique for improving the speed of a program. The potential cutoff sphere, of radius r_{cut}, around a particular atom is surrounded by a 'skin', to give a larger sphere of radius r_{list}. At the first step in a simulation, a list is constructed of all the neighbors of each atom, for which the pair separation is within r_{list}. Over the next few MD time steps, only pairs appearing in the list are checked in the force routine. From time to time the list is reconstructed: it is important to do this before any unlisted pairs have crossed the safety zone and come within interaction range. It is possible to trigger the list reconstruction automatically, if a record is kept of the distance travelled by each atom since the last update. The choice of list cutoff distance rlist is a compromise: larger lists will need to be reconstructed less frequently, but will not give as much of a saving on CPU time as smaller lists. This choice can easily be made by experimentation.

For larger systems ($N \geq 1000$ or so, depending on the potential range) another technique becomes preferable. The cubic simulation box (extension to non-cubic cases is possible) is divided into a regular lattice of $n_{cell} \times n_{cell} \times n_{cell}$ cells. These cells are chosen so that the side of the cell $l_{cell} = L/n_{cell}$ is greater than the potential cutoff distance r_{cut}. If there is a separate list of atoms in each of those cells, then searching through the
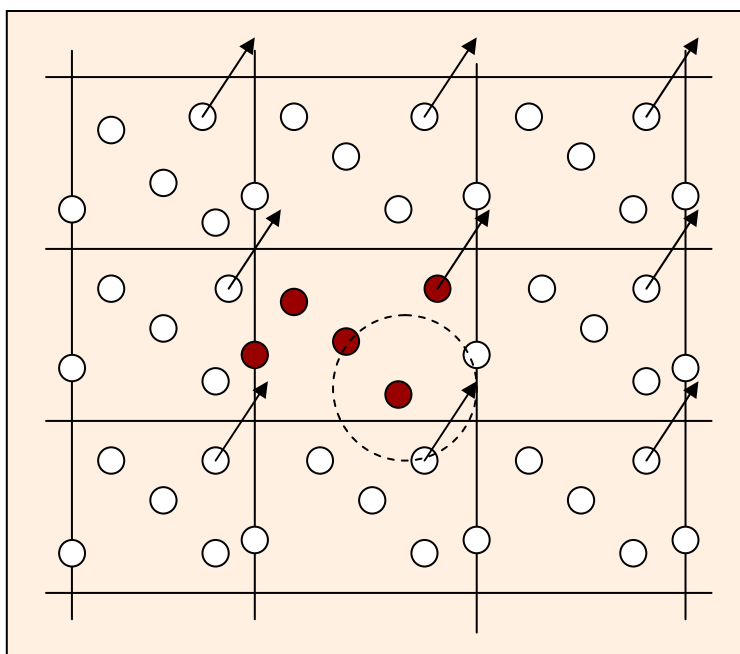
Fig 6.2 Periodic boundary conditions.

neighbours is a rapid process: it is only necessary to look at atoms in the same cell as the

atom of interest, and in nearest neighbour cells. The cell structure may be set up and used

by the method of linked lists. The first part of the method involves sorting all the atoms

into their appropriate cells. This sorting is rapid, and may be performed every step. Then,

within the force routine, pointers are used to scan through the contents of cells, and

calculate pair forces. This approach is very efficient for large systems with short-range

forces. A certain amount of unnecessary work is done because the search region is cubic,

not (as for the Verlet list) spherical.

6.9 Direct velocity scaling

Direct velocity scaling is a drastic way to change the velocities of the atoms so that

the target temperature can be exactly matched whenever the system temperature is higher

or lower than the target by some user-defined amount. Direct velocity scaling cannot be

used to generate realistic thermodynamic ensembles, since it suppresses the natural fluctuations of a system. It can be used to bring a system to equilibrium quickly, at which point a more appropriate thermostat can be used. In Materials Studio, the velocities of all atoms are scaled uniformly as follows:

$$\left(\frac{v_{new}}{v_{old}}\right)^2 = \frac{T_{target}}{T_{system}}$$

(6.14)

Direct temperature scaling adds (or subtracts) energy from the system efficiently, but it is important to recognize that the fundamental limitation to achieving equilibrium is how rapidly energy can be transferred to, from, and among the various internal degrees of freedom of the structure. The speed of this process depends on the energy expression, the parameters, and the nature of the coupling between the vibrational, rotational, and translational modes. It also depends directly on the size of the system, larger systems taking longer to equilibrate. Velocity increments to attain desired temperature governed by the relationship

$$\frac{1}{2}mv^2 = \frac{3}{2}NK_bT$$

(6.15)

Maxwell Boltzmann distribution (probability) is used to guess the velocity for a timestep.

6.10 Forcite Module

Forcite is a molecular mechanics module for potential energy and geometry optimization calculations of arbitrary molecular and periodic systems using classical mechanics. Forcite offers support for the PCFF force fields. With this wide range of force-fields, Forcite can handle essentially any material. The geometry optimization algorithm

offers steepest descent, conjugate gradient, and quasi-Newton methods, in addition to the Smart algorithm, which uses these methods sequentially. This allows very accurate energy minimizations to be performed.

A standard constant stress molecular dynamics (MD) simulation method was applied to construct the atomistic models of the polymer/CNT composites in this study by setting up an appropriate inter-atomic potential function (specified in the following discussion). MD simulations are useful to study the time evolution behavior of systems in a variety of states where thermal sampling of configurational space is required. After equilibration at finite temperature, an energy minimization method was applied to calculate the elastic moduli of the models structures computed from the MD simulations. Periodic boundary conditions were applied to the models along both the tube axis and transverse directions.

6.11 Results and Discussions

Simulations have been made using FORCITE module of MATERIAL STUDIO software to observe the behavior of nanotubes and nanocomposites under thermal fluctuations and under application of constant strain to get the mechanical properties. NVT Ensemble has been used with velocity verlet scheme for integration with pcff force-field. Further in Figures from 6.3A to 6.6C, we have the list of models simulated under different conditions and the output data from performing minimization and production runs.
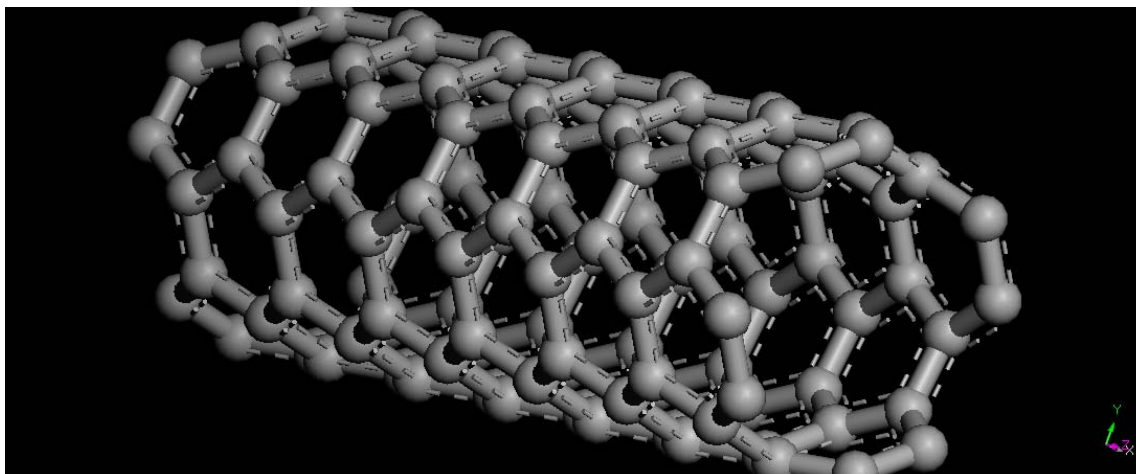
Fig 6.3A SWNT Armchair (4,4) with D=5.42 Å and L=17.216585 Å at T=298K
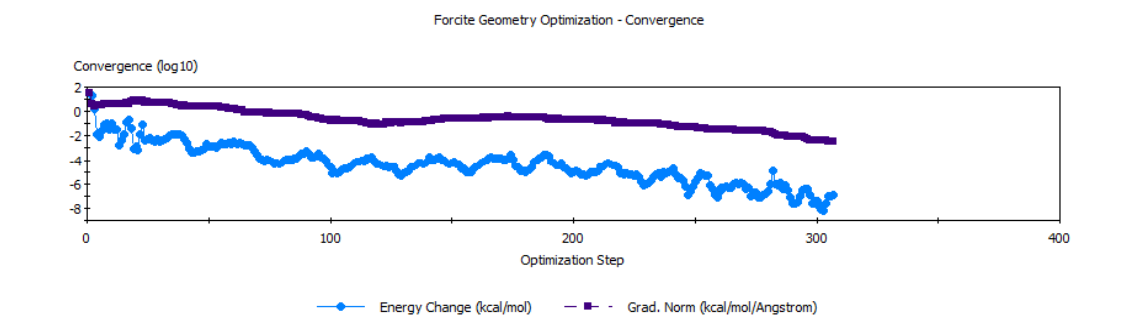

Fig 6.3B Convergence of SWNT Armchair (4,4) during geometry optimization

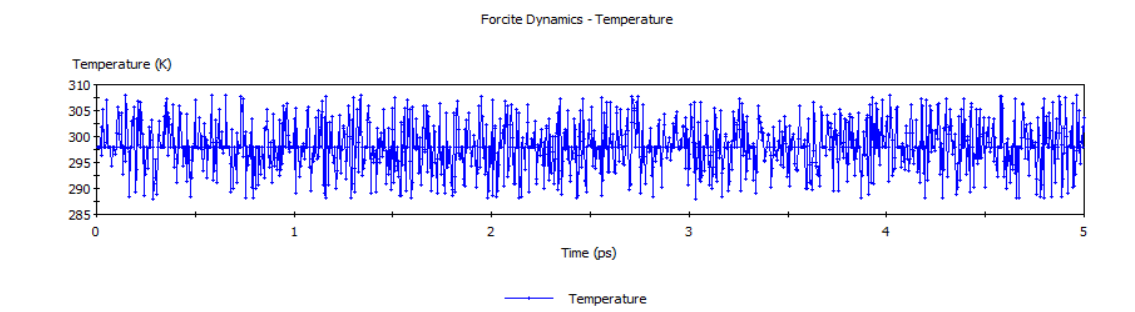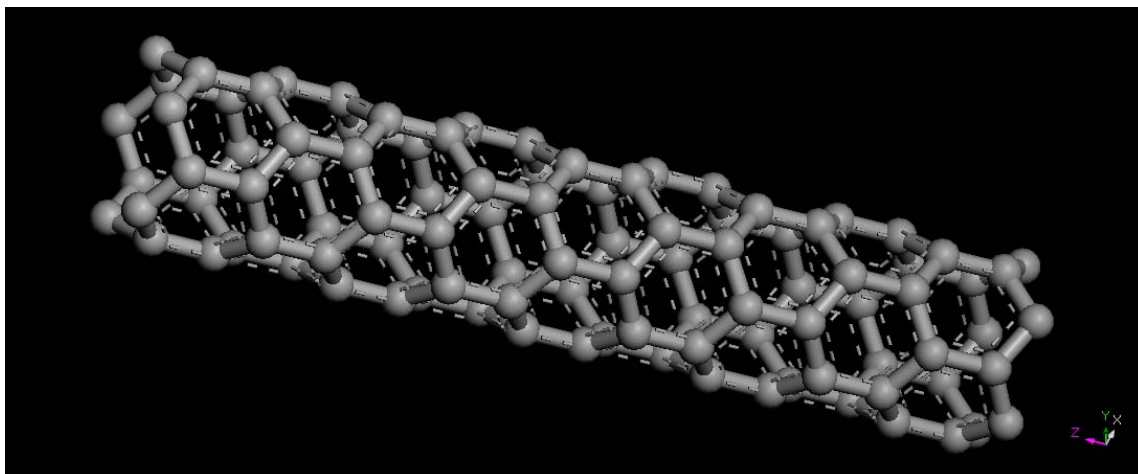**Fig 6.3C Temperature deviation during the dynamics run for   SWNT Armchair (4,4)**

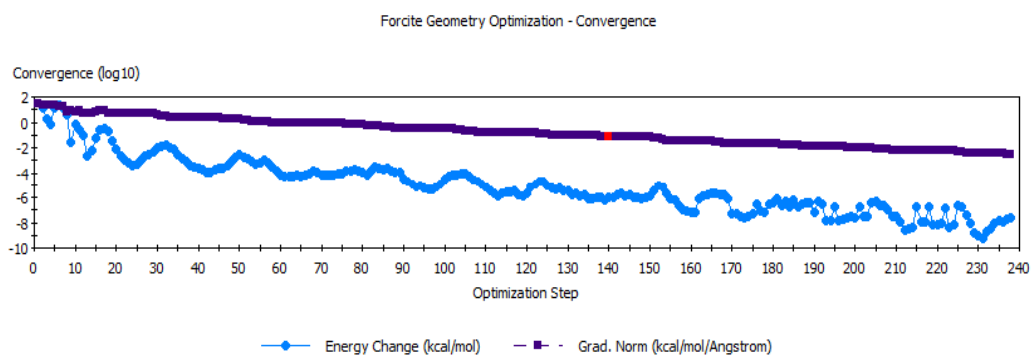**Fig 6.4A SWNT Zigzag (5,0) with D=3.91A and L=21.3A at T=298K**

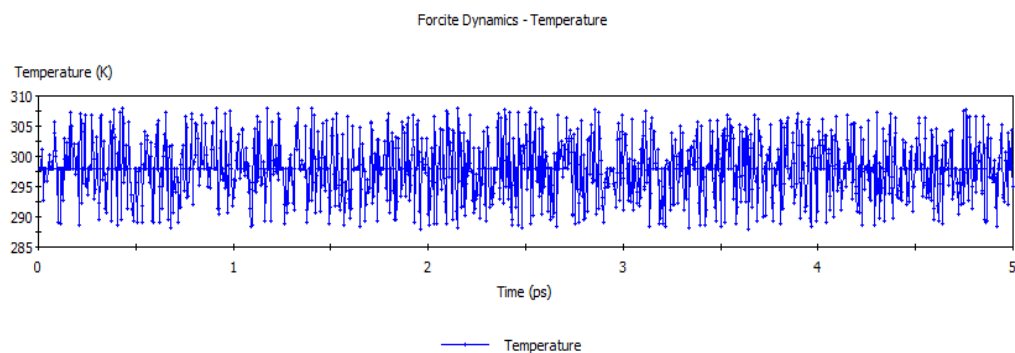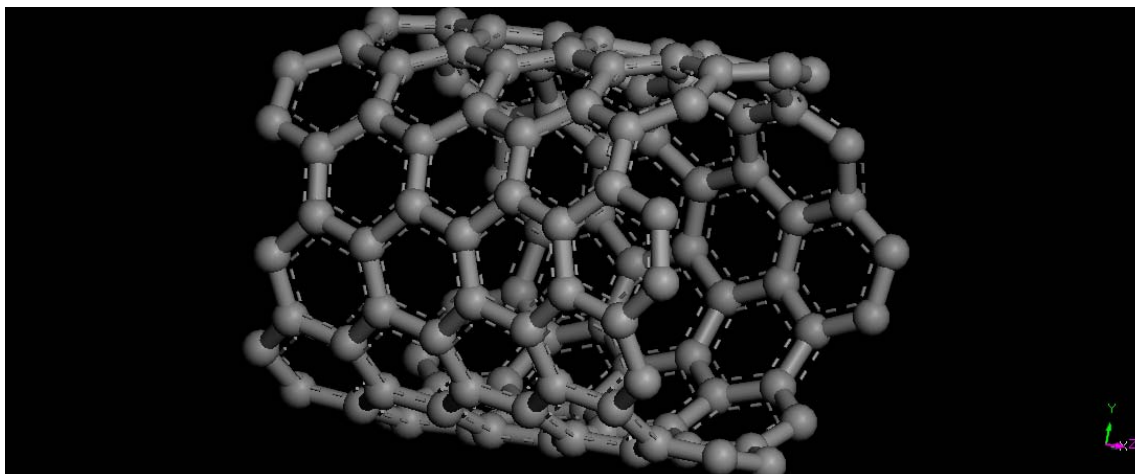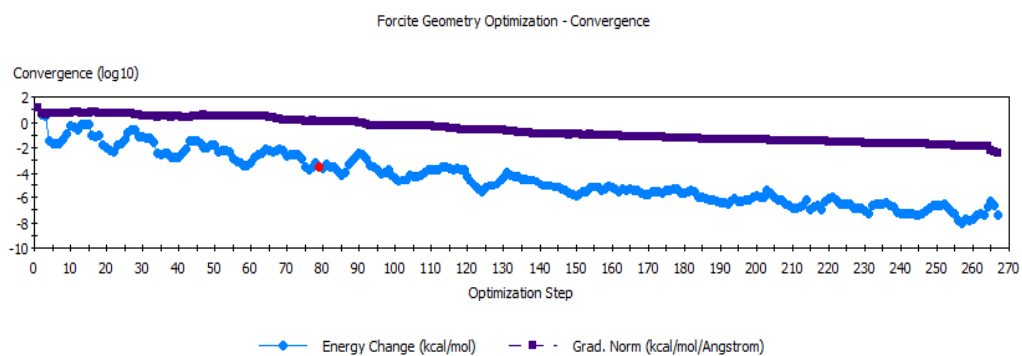**Fig 6.4B Convergence of SWNT Zigzag (5,0) during geometry optimization**

Fig 6.4C Temperature deviation during the dynamics run for SWNT Zigzag (5,0)

Fig 6.5A SWNT Chiral (4,8) with D=8.29Å and L=11.270901 Å

Fig 6.5B Convergence of SWNT Chiral (4,8) during geometry optimization

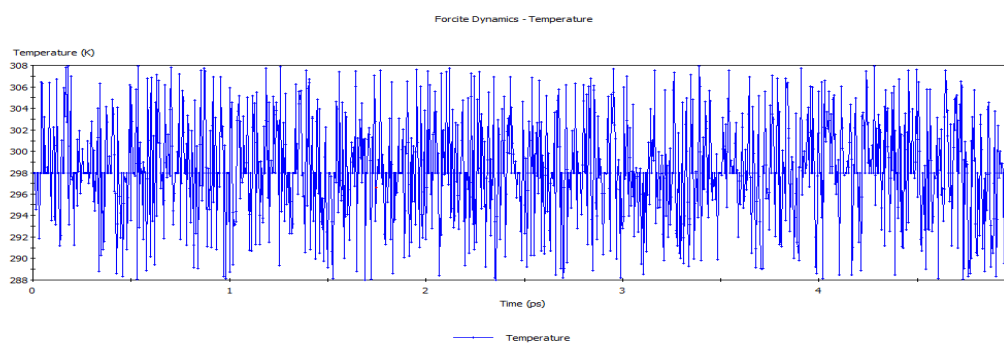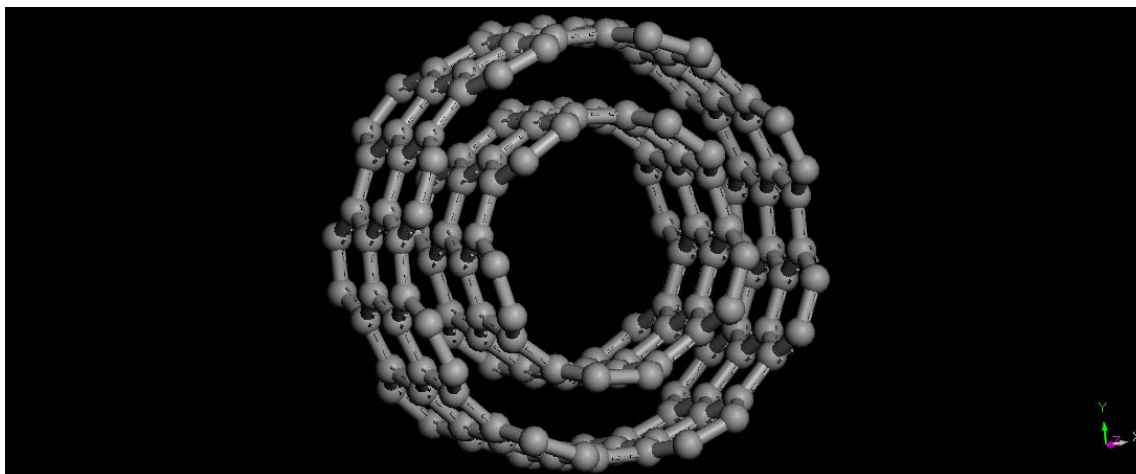**Fig 6.5C Temperature deviation during the dynamics run for SWNT Chiral (4,8)**

Fig 6.6A DWNT with (8,8) as D0=10.85 Å, (5,5) as Di=6.78 Å and L=7.38 Å
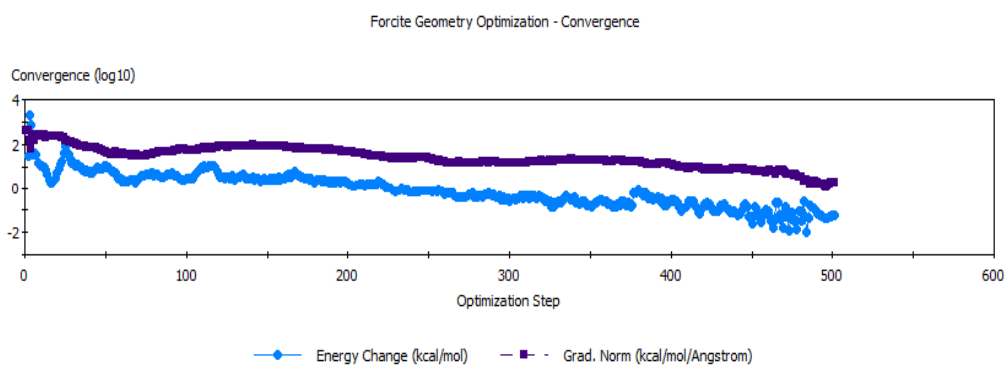

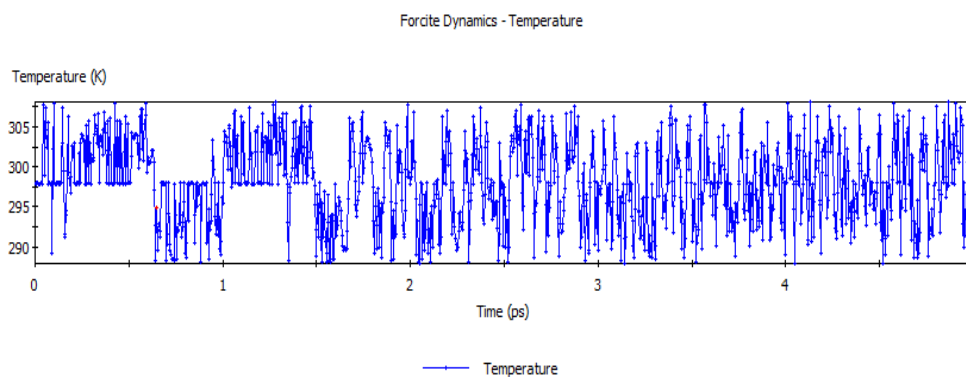**Fig 6.6B Convergence of DWNT (5,5) -(8,8) during geometry optimization**

Fig 6.6C Temperature deviation during the dynamics run for DWNT (5,5) -(8,8)

Now in figures 6.7- 6.15 shown below, we have the plots of E and G for the above specimens of SWNTs and DWNTs to analyze their variation with length and diameter. The mechanical properties are obtained using Forcite module in Materials Studio. We will therefore be in a position to make a comparative study of the results obtained from FE method and MD simulations.

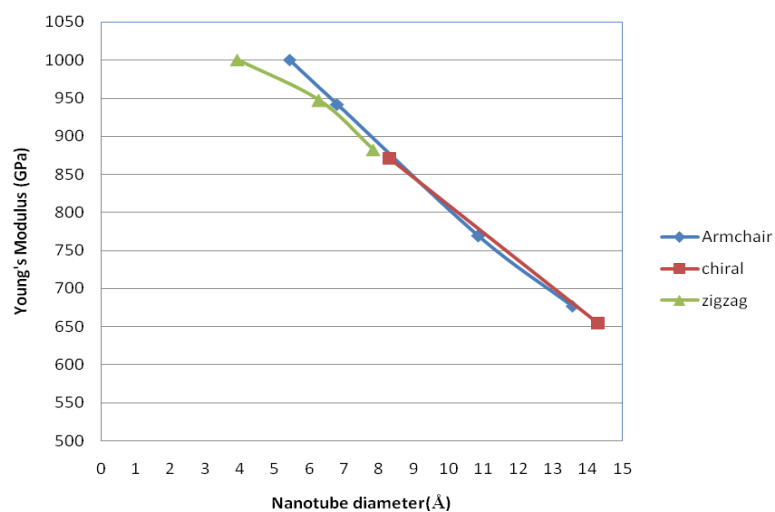**Fig 6.7 Variation of Young's modulus with nanotube diameter**
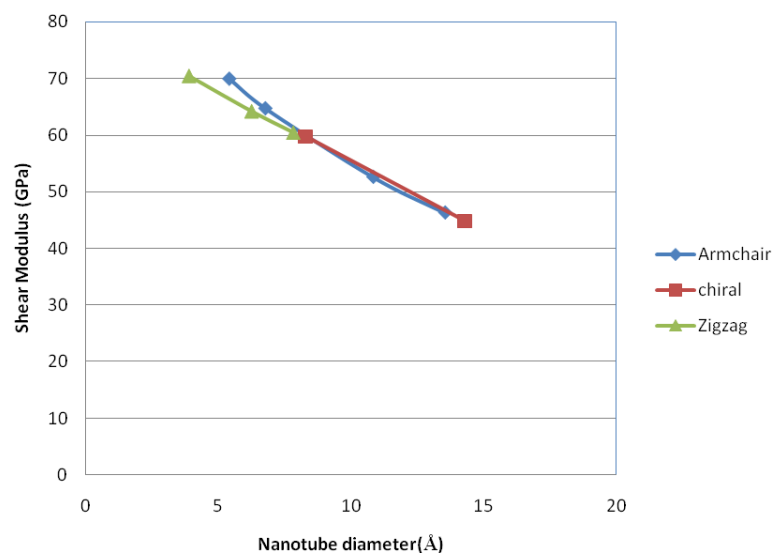

Fig 6.8 Variation of Shear modulus with nanotube diameter
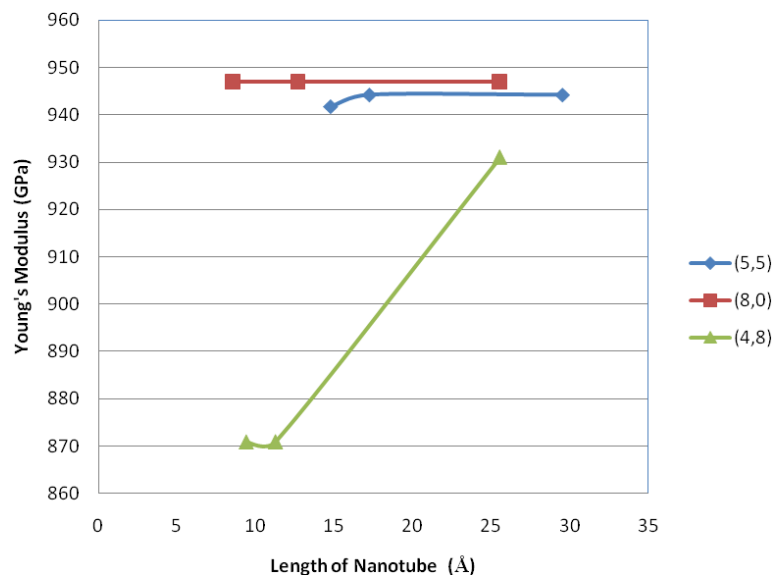
Fig 6.9 Variation of Young's modulus with nanotube length

Fig 6.10 Variation of Shear modulus with nanotube length

Fig 6.11 Variation of Young's modulus with Strain applied at the ends of the nanotube

Fig 6.12 Variation of Young's modulus with outer diameter of double walled nanotube

Fig 6.13 Variation of Shear modulus with outer diameter of double walled nanotube

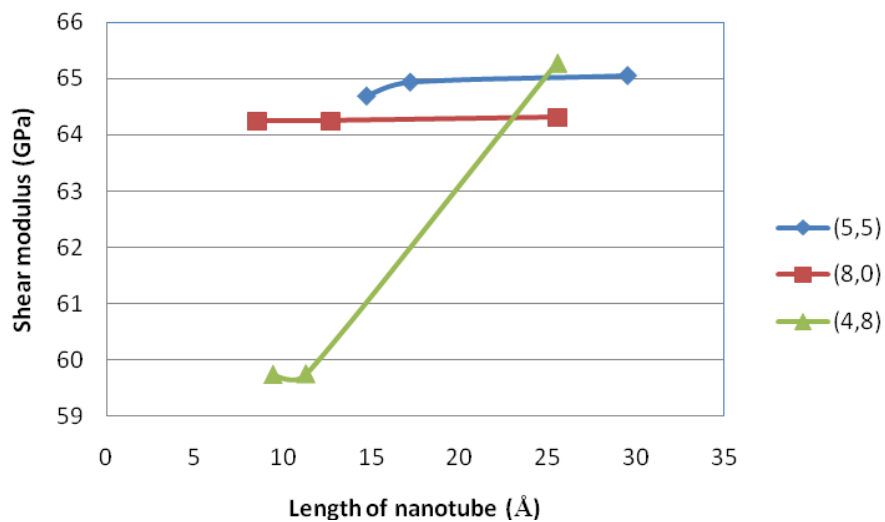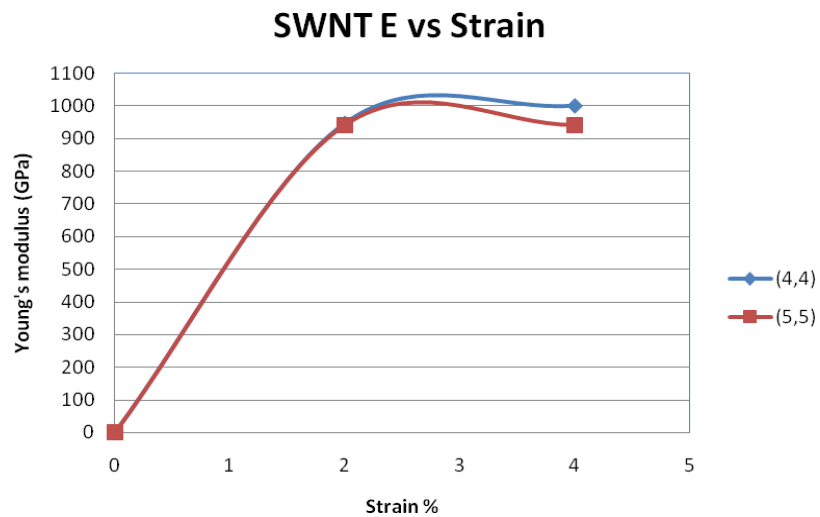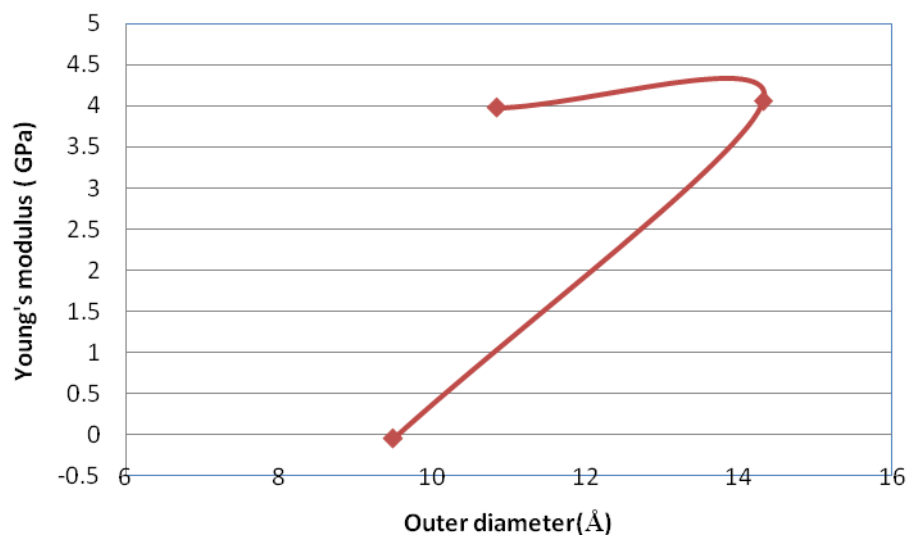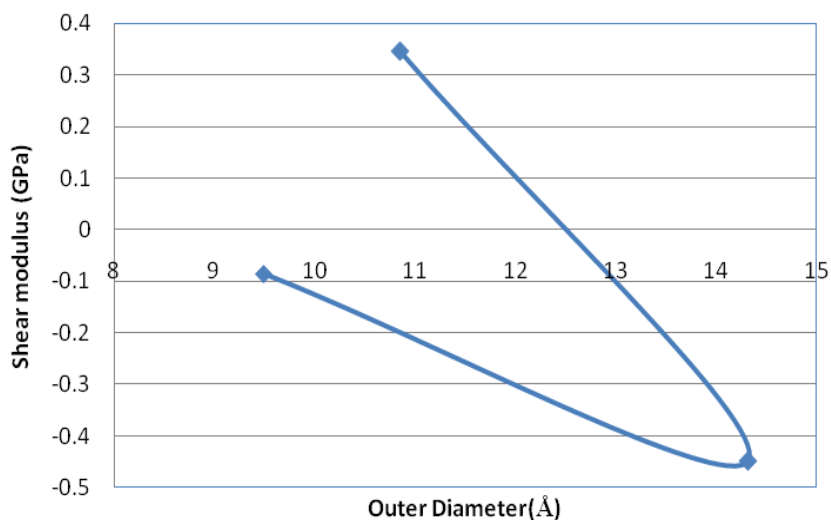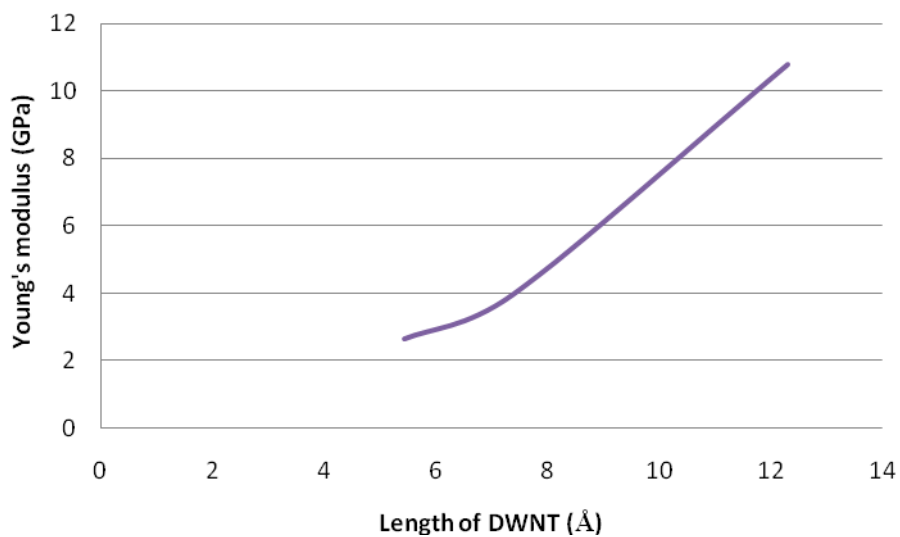**Fig 6.14 Variation of Young's modulus with DW nanotube length**
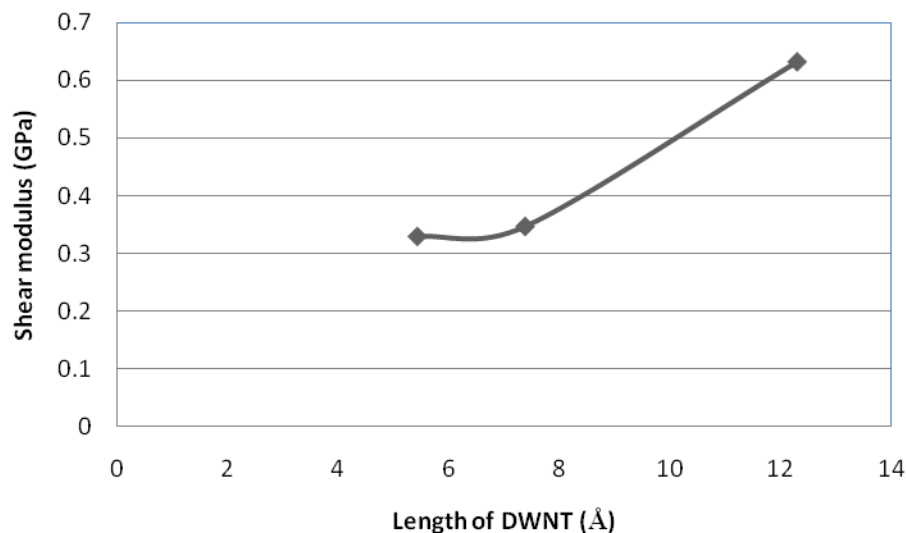
Fig 6.15 Variation of Shear modulus with DW nanotube length

Next we present classical molecular dynamics (MD) simulations of model polymer/CNT composites constructed by embedding a single wall (10, 10) CNT into two different amorphous polymer matrix of poly-oxyacetylene as shown in Fig 6.16 with different volume fractions. A constant-strain energy minimization method was then applied to calculate the axial and transverse elastic moduli of the composite system.

In general, semi-crystalline thermoplastic polymers can exhibit relatively large strains compared to other amorphous materials in which only a small elastic strain can be generated before either fracture or yielding takes place. Since the ultimate tensile strength or yield stress are governed by the presence of defects, then the large-scale microstructure of the material is more pertinent than the local atomic structure. Hence it is computationally very difficult to calculate the strength of pure polymer systems, and also in composite systems undergoing large plastic deformations (e.g. fibre pull-out) using the molecular dynamics method. It is for this reason that the current study focuses on the calculation of low strain

elastic moduli only, with the principle motivation being an elucidation of the effect of interfacial interaction energy between CNTs and polymer matrices on the elastic moduli of their composites. However, it is certain that these interfacial phenomena will also affect the strength of the composite.
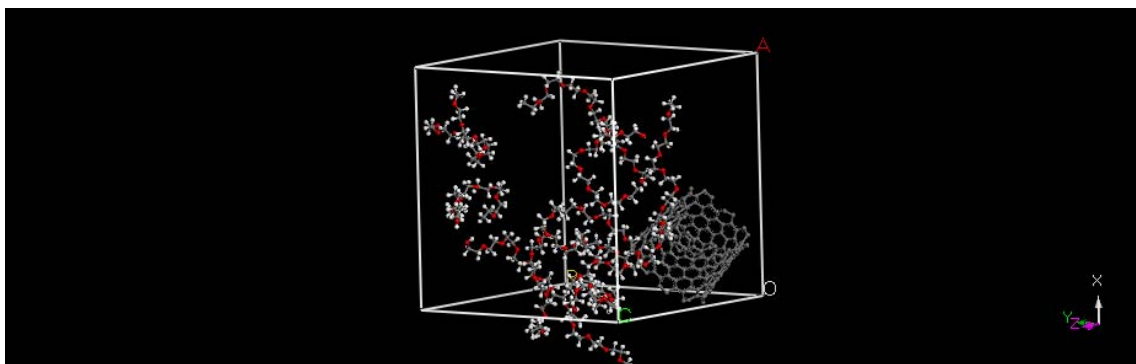

Fig 6.16A Minimized configuration of (10, 10) SWNT in poly-oxyacetylene matrix of 10 chains in the cell
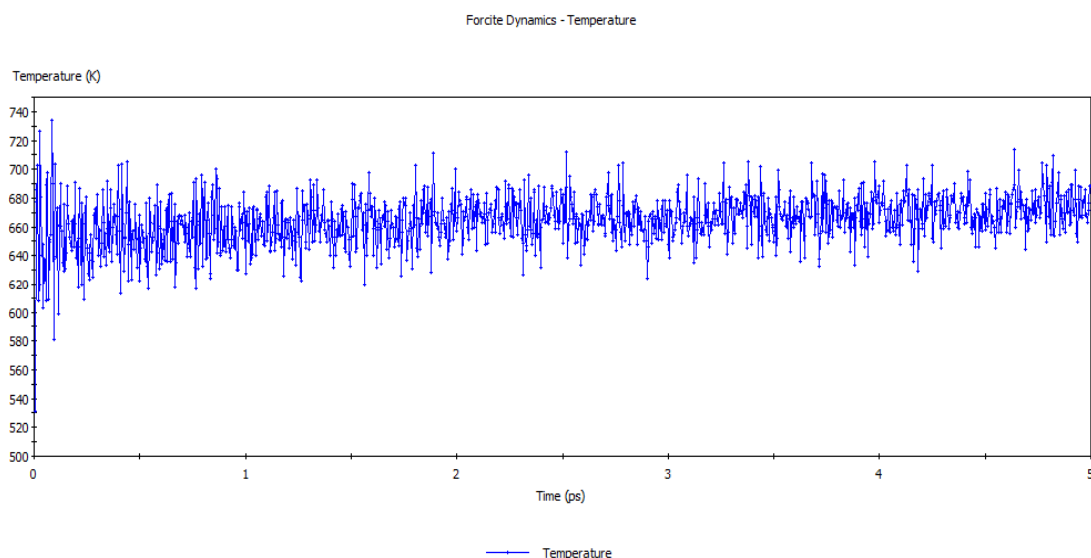

Fig 6.16B Temperature window of (10, 10) armchair SWNT in poly-oxyacetylene

Table 6.1 Elastic stiffness constants *Cij* (GPa), $\sigma_i=C_{ij}\varepsilon_j$, for an applied strain of 0.002

C_{ij}	1	2	3	4	5	6
1	-0.2693	0.6596	-0.5334	0.613	0.1219	0.2005
2	0.6596	-0.7092	-0.2432	0.2944	0.5259	0.1712
3	-0.5334	-0.2432	1.6638	0.3261	-0.1121	-0.1704
4	0.613	0.2944	0.3261	0.6425	-0.5957	-0.0083
5	0.1219	0.5259	-0.1121	-0.5957	0.3728	-0.4341
6	0.2005	0.1712	-0.1704	-0.0083	-0.4341	-0.0231

Table 6.2 Elastic stiffness constants *Cij* (GPa), $\sigma_i=C_{ij}\varepsilon_j$, for an applied strain of 0.004

C_{ij}	1	2	3	4	5	6
1	-0.4095	0.2271	0.5587	0.0971	-0.1483	-0.1744
2	0.2271	0.0906	0.5354	0.708	0.2728	0.1185
3	0.5587	0.5354	0.9119	0.1802	0.1852	-0.0308
4	0.0971	0.708	0.1802	0.2373	0.0846	-0.0917
5	-0.1483	0.2728	0.1852	0.0846	0.4576	0.1323
6	-0.1744	0.1185	-0.0308	-0.0917	0.1323	-0.2302

Table 6.3 Elastic moduli of nanocomposite for different applied strains

Strain	0.002			0.004		
Elastic Properties	Reuss	Voight	Hill	Reuss	Voight	Hill
Bulk modulus (GPa)	0.0000	0.0501	0.0251	1.5581	0.3595	0.9588
Shear modulus (GPa)	0.0000	0.2519	0.1260	0.0000	0.0444	0.0222
Compressibility (1/TPa)	-15996.3209			641.8113		
λ^* (GPa)	-0.4330			0.3307		
μ^* (GPa)	-0.1122			0.1549		

From the data in tables 6.1, 6.2 and 6.3, we observe that the Shear modulus decreases with increase in strain and Young's modulus in the direction of strain increases with strain. Close observations of the above results obtained using MD simulations subsequently processed using statistical mechanics are likely to lead us to several important conclusions which correlate atomistic scale to macroscale nanocomposites.

CHAPTER VII

SUMMARY AND CONCLUSIONS

7.1 Summary

The discovery of carbon nanotubes has initiated a number of scientific investigations to explore their unique properties and potential applications. They are considered as ideal reinforcements for structural and multifunctional composite applications. However, some crucial issues must be solved before the full potential of carbon nanotubes is realized in the nanocomposite materials. Fundamental understanding and highly accurate predictive methods for the interfacial bonding and mechanical behavior of carbon nanotube/polymer composites are crucial to realize successfully the extraordinary properties of this new class of nanocomposite materials. This part of research has compared different computational methods to study the behavior of nanotubes when subjected to bending, stretching and twisting. Subsequently, one can understand the interfacial bonding and mechanical behavior of carbon nanotube/polymer composites. The comparison sheds light on the main differences and similarities between the methods and introduces the essential features of new methods.

7.2 Conclusions

1) A finite element model using 3D ELASTIC BEAM elements has been presented for studying the behavior of single walled carbon nanotubes under mechanical loading (bending, stretching and twisting).

2) A finite element code has been developed to model multi-walled carbon nanotubes and to impart Van der Waal's forces between adjacent layers and consequently study its effect on the mechanical properties.

3) Parametric studies have been made to analyze the effect on different parameters like diameter, length and wall thickness on the elastic moduli using FE method and MD simulation technique.

4) Contrasting effect of tube diameter on young's modulus of nanotube is observed using 'Finite Element Technique based on Molecular Mechanics' and 'Molecular Dynamics' which is as expected due to the difference in inter-atomic potentials considered at 0 K and higher temperatures.

5) Multi-scale modeling of nanocomposite is presented to study the buckling behavior of carbon nanotube/polymer composite.

6) Elastic constants of carbon nanotube in poly-oxyacetylene matrix are derived using MD to study their variation with density (no. of nanotubes embedded/unit cell volume) of the nanocomposite.

7.3 Scope of Future Work

This work can be extended to determine the mechanical properties of Si_3N_4 and BN nanotubes as well as defective nanotubes and functionalized nanotubes. New models can be suggested to determine the electrical and electronic properties of nanotubes at high temperature.

REFERENCES

[1] S. Iijima, Helical microtubules of graphitic carbon, Nature 354 (1991) 56-58.

[2] M. M. J. Treachy, T. W. Ebbesen, J. Gibson, Exceptionally high Young's modulus observed for individual carbon nanotubes, Nature 381(20) (1996) 678-680.

[3] E. W. Wong, P.E. Sheeshan, C.M. Lieber, Nanobeam mechanics: Elasticity, strength and toughness of nanorods and nanotubes, Science 277 (1997) 1971-1975.

[4] T.W. Tombler, C. Zhou, L. Alexseyev, J. Kong, H. Dai, L. Liu, C. S. Jayanthi, M. Tang, S.Y. Wu, Reversible electromechanical characteristics of carbon nanotubes under local-probe manipulation, Nature 405 (2000) 769-772.

[5] M.F. Yu, O. Lourie, M. J. Dyer, K. Moloni, T.F. Kelly, R.S. Ruoff, Strength and breaking mechanism of multi-walled carbon nanotubes under tensile load, Science 287 (2000) 637-640.

[6] M. R. Falvo, G. J. Clary, R. M. Taylor II, V. Chi, F. P. Brooks Jr., S. Washbum, and R. Superfine, Bending and buckling of carbon nanotubes under large strain, Nature 389 (1997) 582-584.

[7] A. Krishnan, E. Dujardin, T. W. Ebbesen, P. N. Yianilos, and M. M. J. Treacy, Young's modulus of single-walled nanotubes, Phys. Rev. B 58 (1998) 14013-14019.

[8] S. Shen, S. N. Atluri, Atomic-level stress calculation and continuum-molecular system equivalence, CMES: Computer Modeling in Engineering and Science 6 (2004) 91-104.

[9] B. I. Yakobson, C.J. Brabec, J. Bernholc, Nanomechanics of carbon tubes: Instabilities beyond linear response, Phys. Rev. Lett. 76 (14) (1996) 2511-2514.

[10] J. P. Lu, Elastic properties of carbon nanotubes and nanoropes, Phys. Rev. Lett. 79 (7) (1997) 1297-1300.

[11] J. P. Yao, V. Lordi, Young's modulus of single-walled carbon nanotubes, J. Appl. Phys. 84 (4) (1998) 1939-1943.

[12] E. Hernández, C. Goze, P. Bernier, A. Rubio, Elastic properties of C and BxCyNz composite nanotubes, Phys. Rev. Lett. 80 (20) (1998) 4502-4505.

[13] Y. Jin, F.G. Yuan, Simulation of elastic properties of single-walled carbon nanotubes, Composites Science and Technology 63 (2003) 1507-1515.

[14] B.W. Xing, Z.C. Chun, C.W. Zhao, Simulation of Young's modulus of single-walled carbon nanotubes by molecular dynamics, Physica B 352 (2004) 156–163.

[15] K.M. Liew, X.Q. He, C.H. Wong, On the study of elastic and plastic properties of multi-walled carbon nanotubes under axial tension using molecular dynamics simulation, Acta Materialia 52 (2004) 2521–2527.

[16] G. H. Gao, T. Cagin, W. A. Goddard, Energetics, structure, mechanical and vibrational properties of single-walled carbon nanotubes, Nanotechnology 9 (1998) 184-191.

[17] G. V. Lier, C. V. Alsenoy, V. V. Doren, P. Geerlings, 2000. Ab intitio study of the elastic properties of single-walled carbon nanotubes and graphene, Chemical Physics Letters 326 (2000) 181-185.

[18] G. Zhou, W. Duan, B. Gu, First-principles study on morphology and mechanical properties of single-walled carbon nanotube, Chemical Physics Letters 333 (2001) 344-349.

[19] C.Q. Ru, Effect of van der Waals forces on axial buckling of a double walled carbon nanotube, J. Appl. Phys. 87 (10) (2000) 7227-7231.

[20] G. M. Odegarda, T.S. Gatesb, L.M. Nicholsonc, K.E. Wise, Equivalent-continuum modeling of nano-structured materials, Composites Science and Technology 62 (2002) 1869-1880.

[21] C. Li, T.W. Chou, Elastic moduli of multi-walled carbon nanotubes and the effect of van der Waals forces, Composites Science and Technology 63 (2003) 1517– 1524.

[22] C. Li, T.W. Chou, A structural mechanics approach for the analysis of carbon nanotube, International Journal of Solids and Structures 40 (2003) 2487-2499.

[23] C. Li, T.W. Chou, Vibrational behavior of multiwalled carbon-nanotube-based nanomechanical resonators, Appl. Phys. Lett. 84 (121) (2004) 121-123.

[24] C. Li, T.W. Chou, Modeling of elastic buckling of carbon nanotubes by molecular structural mechanics approach, Mechanics of Materials 36 (2004) 1047-1055.

[25] T. Changa, H. Gao, Size-dependent elastic properties of a single-walled carbon nanotube via a molecular mechanics model, J. Mech. Phys. Solids 51 (2003) 1059 – 1074.

[26] T. Natsuki, K. Tantrakarn, M. Endo, Effects of carbon nanotube structures on mechanical properties, Appl. Phys. A 79 (2004) 117-124.

[27] T. Natsuki, M. Endo, Stress simulation of carbon nanotubes in tension and compression, Carbon 42 (2004) 2147-2151.

[28] T. Natsuki, K. Tantrakarn, M. Endo, Prediction of elastic properties for single-walled carbon nanotubes, Carbon 42 (2004) 39-45.

[29] H.W. Zhang, J.B. Wang, X. Guo, Predicting the elastic properties of single-walled carbon nanotubes, J. Mech. Phys. Solids 53 (2005) 1929–1950.

[30] J.R. Xiao, B.A. Gama, J.W. Gillespie, An analytical molecular structural mechanics model for the mechanical properties of carbon nanotubes, International Journal of Solids and Structures 42 (2005) 3075–3092.

[31] K.T. Lau, M. Chiparab, H.Y. Linga, D. Hui, On the effective elastic moduli of carbon nanotubes for nanocomposite structures, Composites: Part B 35 (2004) 95-101.

[32] X. Sun, W. Zhao, Prediction of stiffness and strength of single-walled carbon nanotubes by molecular-mechanics based finite element approach, Materials Science and Engineering A 390 (2005) 366–371.

[33] K.I. Tserpes, P. Papanikos, Finite element modeling of single-walled carbon nanotubes, Composites: Part B 36 (2005) 468-477.

[34] M. Meo, M. Marco Rossi, Prediction of Young's modulus of single wall carbon nanotubes by molecular-mechanics based finite element modeling, Composites Science and Technology 66 (2006) 1597–1605.

[35] A.L. Kalamkarov, A.V. Georgiades, S.K. Rokkam, V.P. Veedu, M.N. Ghasemi-Nejhad, Analytical and numerical techniques to predict carbon nanotubes properties, International Journal of Solids and Structures 43 (2006) 6832–6854.

[36] G.I. Giannopoulos, P.A. Kakavas, N.K. Anifantis, Evaluation of the effective mechanical properties of single walled carbon nanotubes using a spring based finite element approach, Computational Material Science 41 (2008) 51-569.

[37] 3-D Elastic Beam, http://sc.tamu.edu/softwareDocs/ansys80/Hlp_E_BEAM4.html Accessed on 6/2008.

[38] C. Li, T.W. Chou, Multiscale modeling of compressive behavior of carbon nanotube/polymer composites, Composites Science and Technology 66 (2006) 2409-2414.

[39] M. S. Dresselhaus, G. Dresselhaus, and R. Saito, Physics of Carbon Nanotubes, Carbon 33 (7) (1995) 883–891.

[40] J.N. Reddy, An Introduction to Nonlinear Finite Element Analysis, Oxford University Press: Oxford, U.K. 2004.

[41] J.N. Reddy, An Introduction to the Finite Element Method, McGraw-Hill, New York. 2006.

VITA

Dhatri Gaddamanugu received her Bachelor of Engineering degree in mechanical engineering from Osmania University, Hyderabad, India in 2006. She entered the master's program in mechanical engineering at Texas A&M University in January 2007 and received her Master of Science degree in May 2009. Her research interests include structural mechanics, finite element methods in solid mechanics. She plans to do her Doctor of Philosophy degree in biomechanics, multi-scale methods and nanomechanics.

Ms. Dhatri may be reached at Advanced Computational Mechanics Laboratory, Wisenbaker Engineering Research Center 159, Texas A&M, College Station, TX 77840. Her email is dhatrig17@gmail.com.